

Vertical Transport Timescale of Surface-Produced Particulate Material in the Chesapeake Bay

 Jilian Xiong¹  and Jian Shen¹ 
¹Virginia Institute of Marine Science, William & Mary, Gloucester Point, VA, USA

Key Points:

- The vertical particulate age (VPA) explains the time lag between the springtime algae blooms and the summertime hypoxia in the bay
- Long resting of particulates on the seabed and resuspension of the aged seabed material largely elongate the VPA in the water column
- The VPA is sensitive to settling velocity and episodic freshwater pulse. The latter entrains old material from shoals to the deep channel

Supporting Information:

Supporting Information may be found in the online version of this article.

Correspondence to:

 J. Xiong,
jxiong@vims.edu;
xiongjilian@gmail.com
Citation:

 Xiong, J., & Shen, J. (2022). Vertical transport timescale of surface-produced particulate material in the Chesapeake Bay. *Journal of Geophysical Research: Oceans*, 127, e2021JC017592. <https://doi.org/10.1029/2021JC017592>

Received 19 MAY 2021

Accepted 22 JAN 2022

Abstract Accumulation and remineralization of surface-produced particulate organic matter (POM) in the water column and seabed link closely to hypoxia and the health of aquatic ecosystems. The POM retention time provides a key timescale to interpret biochemical reaction processes. In this study, we investigated the spatiotemporal variations in the vertical particulate age (VPA) of surface-produced POM, which is the mean time elapsed since the particulates last contact the surface, by incorporating major physical processes including sinking, resuspension, and deposition in the Chesapeake Bay. It was found that the vertical transport time for the particulates (i.e., VPA) is much longer than the dissolved counterparts as the former consists of new material from the surface and the resuspended aged material that has elongated resting on the seabed after deposition. The VPA is sensitive to settling velocity, especially in low-frequent resuspension environments, and varies over 2 orders of magnitude with settling velocity from 0 to 10 m/day. Slow-sinking material can remain in suspension and seldom settle to the seabed, thus mainly contribute to pelagic processes, while the fast-sinking material connects closely with benthic processes. The seasonality of VPA decreases as the settling velocity increases. No significant difference in VPA was found between wet and dry years, yet the episodic strong flood events entrain old materials from the depositional lateral shoals to increase VPA in the channel. The transport age bridges cross disciplinary by providing the fourth-dimensional age information as a common currency to compare the physical transport timescale with the timescales for biochemical reactions.

Plain Language Summary The Chesapeake Bay is a highly productive estuary, characterized by spring phytoplankton blooms and subsequent accumulations of particulate organic matter (POM) in the bottom layer, which fuels summertime hypoxia. The retention time of POM provides an important timescale to interpret biochemical reactions in estuaries. In this study, we applied the vertical particulate age (VPA), the average time elapsed since the POM leaving the surface, to estimate the downward-transport time. The VPA accounts for all possible trajectories, including direct sinking and interactions with the seabed via resuspension and deposition. It was found that the VPA is much longer than the vertical transport time for dissolved material due to the elongated resting of particulates on the seabed and contributions from the resuspended old material. The VPA is sensitive to the settling velocity and increases 2 orders of magnitude with the settling velocity from 0 to 10 m/day in less dynamic environments. The slow-sinking material can remain in suspension while the fast-sinking material mostly stays on the seabed. No significant difference in the VPA was found between wet and dry years except during the episodic freshwater pulse, which brought aged materials from the depositional shoals to increase the VPA in the channel.

1. Introduction

Estuaries are of major significance for organic matter (OM) production, cycling, and export to the coastal ocean (Canuel & Hardison, 2016; McCallister et al., 2006; Raymond & Bauer, 2001a). Accumulation and decomposition of OM in the bottom deep trench are closely related to hypoxia and thus impact the health of aquatic ecosystems. The OM that fuels the oxygen consumption may originate from the watershed, that is, allochthonous source, such as vascular plant detritus, soil leaching and erosion, and agriculture runoff, or from the settled phytoplankton production within the system, that is, autochthonous source (Autoc-OM), such as senescent cells, zooplankton fecal pellets, and marine aggregates (Rabalais et al., 2010).

The amount of consumption and transformation of OM in an estuary increases with the residence time. For example, the long residence time (~180 days; Du & Shen, 2016) associated with the bathymetry-induced strong water reflux (Xiong et al., 2021a) can result in high retention of nutrients and OM in the middle reach of the Chesapeake Bay (CB), promoting high rates of internal Autoc-OM production (Fennel & Testa, 2019) and respiration

© 2022 The Authors.

 This is an open access article under the terms of the [Creative Commons Attribution-NonCommercial License](https://creativecommons.org/licenses/by-nc/4.0/), which permits use, distribution and reproduction in any medium, provided the original work is properly cited and is not used for commercial purposes.

(Du & Shen, 2015; Kemp et al., 1992), and further developing the recurring summertime hypoxia and anoxia in the deep central basin (Murphy et al., 2011). Accumulating evidence suggests the connection between the deposition of springtime OM to sediments and the summertime oxygen depletion in the bottom of CB (Cercio, 2000; Malone et al., 1988; Zheng & DiGiacomo, 2020), yet the specific transport time for the surface-produced OM from the spring phytoplankton blooms to reach the bottom has not been quantified. The transport time is one of the key timescales to interpret the biochemical reaction processes and provides an important linkage between the physical and biochemical processes by placing them in a comparable currency (Lucas & Deleersnijder, 2020; Lucas et al., 2009).

As the phytoplankton species typically shift from the springtime larger diatoms with relatively high sinking rates to the summertime smaller diatoms and other taxa including dinoflagellate, cyanobacteria, chlorophytes, and picophytoplankton (Brush et al., 2020; Malone & Chervin, 1979; Marshal et al., 2006), the organisms with different sinking rates may experience diverse transport pathways and travel times from the surface to the bottom, thus contribute differently to the pelagic and benthic biochemical processes. It is suggested that the springtime diatoms can sink to the benthic layer and probably join the benthic food chains before the formation of the summer thermocline, while the summertime nanoplankton is more vulnerable to grazing thus enters the pelagic food chains before sinking from the surface layer (Malone & Chervin, 1979). Previous investigations indicate that the accumulation of labile OM deposited on the seabed can carry over to the following spring due to low temperature, contributing to the elevated sediment oxygen demand (SOD) and the reduced oxygen concentration in the water column (Brady et al., 2013; Officer et al., 1984; Taft et al., 1980). The content of sedimentary OM also depends on the source and the potential retention efficiency in different environments. For example, the sedimentary OM content is high in the oligohaline and mesohaline CB, as the former receives the fluvial OM while the latter is supported by the sinking of spring phytoplankton blooms (Boynton et al., 2018; Testa et al., 2020). It is, therefore, of interest to estimate the duration for the surface-produced OM to remain in the sediments at different locations with diverse dynamics.

Recently, J. Wang and Hood (2020) implemented a backward Lagrangian particle tracking model to trace the origin of the bottom particulate organic matter (POM) that fuels deep channel hypoxia in the mesohaline CB. The model results suggest that the locally originated POM with high sinking rates is most important in driving oxygen depletion. Nevertheless, the potential interactions between particles and bottom sediments, for example, resuspension and deposition which can elongate the travel distance of the particles, were neglected in their particle tracking model. The benthic-pelagic coupling in shallow coastal environments can regulate the transfer, retention, and recycling of OM and influence the recovery time of eutrophic ecosystems (Boynton et al., 2018; Brady et al., 2013; Testa et al., 2020). The downward transport of OM is a primary mechanism that connects benthic and pelagic habitats (Brady et al., 2013; Z. Wang et al., 2020). Cercio et al. (2010) suggest that deposition of spring diatom blooms to the sediments can provide a significant carbon source to the SOD. The degree to which sediment resuspension and transport affect estuarine biochemistry was quantified by Moriarty et al. (2020). Besides the recognized significance of resuspension and deposition processes on the water column biochemistry, the transport timescale affected by these processes has not been well studied yet.

As the POM leaves the surface layer, it would take multiple trajectories to the bottom and fuel the deep-water oxygen depletion, including direct sinking from the overlying water column (Hagy et al., 2005; Kemp et al., 1997) and indirect sources from the shallow flanks via lateral circulation (Cercio et al., 2013; Malone et al., 1986; Testa & Kemp, 2008; H. Wang, 2020) and from the downstream via gravitational circulation (Malone et al., 1988; Officer et al., 1984). Despite the various pathways, the vertical particulate age (VPA) quantifies the overall time for the downward transport of the surface layer POM to a target location such as the bottom water layer. VPA is defined as the mean time elapsed since the particulates under consideration last contact the surface where the VPA is zero. The general theory of the age for dissolved substances is developed by Delhez et al. (1999) and is widely applied to quantify the transport timescale of water mass, pollutants, and dissolved nutrients in major coastal waterbodies (e.g., de Brye et al., 2012; Deleersnijder et al., 2001; Gustafsson & Bendtsen, 2007; Lucas & Deleersnijder, 2020; Shen & Haas, 2004; Shen & Wang, 2007; Sun et al., 2020; Zhang et al., 2010). Age is defined as the time elapsed since the particle last contacts with its source region (Delhez et al., 1999; Takeoka, 1984). The original Constituent-oriented Age and Residence time Theory (CART; www.climate.be/cart) formulated for dissolved tracer (Delhez et al., 1999) was extended by Mercier and Delhez (2007) to calculate the age of sinking material, featuring settling and interactions with the seabed via resuspension and deposition. The transport age of

particulate material has been successfully used to investigate the river-borne sediment transport in the York River (Gong & Shen, 2010), Hudson River (Ralston & Geyer, 2017), and Pearl River Estuary (Zhu et al., 2020, 2021).

To date, the quantifications of the particulate material transport age are all with sources from the watershed, seldom focusing on the surface-originated sinking material. In the current study, we applied the CART approach to quantify the vertical transport timescale of the surface-produced particulate material (i.e., the VPA) in CB, a large productive estuary on the eastern coast of the United States. The particulates are some combinations of dead or dying phytoplankton, zooplankton remains, fecal pellets, and organic aggregates including the adsorbed dissolved OM (Officer et al., 1984). We mainly place the VPA in an ecological perspective. It measures the mean transport time of particulate material from the surface to a target location as the material may experience different trajectories. As a first step toward the understanding of the vertical transport timescale of particulate material, this study focuses on the influence of physical processes (e.g., advection, settling, resuspension, and deposition), which would differentiate the particulate material transport greatly from the dissolved counterpart. The full coupling of the complicated biochemical reactions associated with the POM and the physical transport into the age algorithms and the potential significance merit further efforts.

This paper is organized as follows. Section 2 described the hydrodynamic model and diagnostic transport age. The results of the VPA and the respective total time spent in the water column and on the seabed for material with various settling velocities were presented in Section 3. The influence of settling velocity, resuspension process, and freshwater discharge on the VPA were discussed in Section 4, with the conclusions were given in Section 5.

2. Methodology

2.1. Hydrodynamic Model

The Environmental Fluid Dynamics Code (EFDC, Hamrick, 1992) was applied to simulate the hydrodynamics and to calculate the transport timescale of particulate material. The present model application in CB has been well-calibrated and reproduces reliable stratification and de-stratification in both wet and dry years (Hong & Shen, 2012). It utilizes a 112 by 224 curvilinear grid in the horizontal dimension with 20 evenly spaced sigma coordinates in the vertical dimension. The model domain includes the major tributaries and the adjacent shelf region (Figure 1a). It is forced by river discharges from USGS observations at nine large tributaries, tides interpolated from three monitoring stations (Lewes, Delaware; CBBT, Virginia; Duck, North Carolina), and winds from the North America Regional Reanalysis. The salinity boundary condition was interpolated from the monthly climatology of World Ocean Atlas 2001 (Boyer et al., 2005). The model is initialized with the long-term mean conditions from the observations by the Chesapeake Bay Program.

The transport equation for a tracer in the water column with settling implemented in the model is similar to that for the suspended sediment and is expressed as

$$\frac{\partial C}{\partial t} + \frac{\partial(Cu)}{\partial x} + \frac{\partial(Cv)}{\partial y} + \frac{\partial C(w - w_s)}{\partial z} = \frac{\partial}{\partial x} \left(K_h \frac{\partial C}{\partial x} \right) + \frac{\partial}{\partial y} \left(K_h \frac{\partial C}{\partial y} \right) + \frac{\partial}{\partial z} \left(K_z \frac{\partial C}{\partial z} \right) \quad (1)$$

where, C [gm^{-3}] is a numerical tracer in the present age study. w_s is the settling velocity [ms^{-1}], which is zero for dissolved material. K_h and K_z are horizontal and vertical diffusivities [m^2s^{-1}], respectively. The velocity field (u , v , w) and the diffusion coefficients are provided by the hydrodynamic module.

At the surface water, no material flux is allowed and the boundary condition is

$$w_s C + \frac{\partial}{\partial z} (K_z C) = 0 \quad (2)$$

The material in the bottom water layer exchanges with the seabed through deposition and resuspension processes,

$$w_s C + \frac{\partial}{\partial z} (K_z C) = D - E \quad (3)$$

where, D and E are the corresponding deposition and resuspension (or erosion) rates. The erosion rate E is calculated as

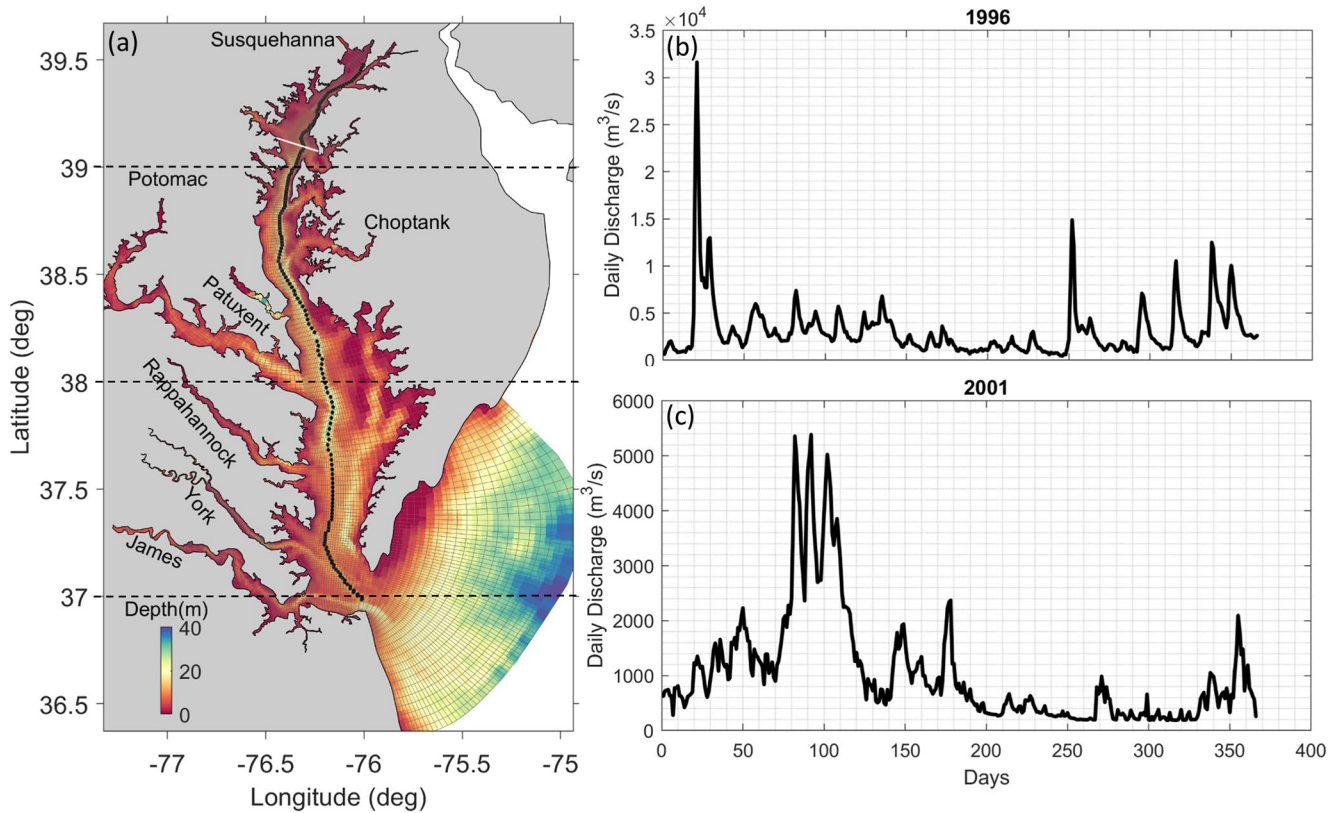


Figure 1. (a) Model grid covering the Chesapeake Bay (CB) and the adjacent continental shelf, with the black dots denoting the location of the main channel and the white line denoting the selected cross-bay section in the upper bay. The mainstem of CB is divided into lower (37–38°N), middle (38–39°N), and upper bay (>39°N). (b) and (c) Daily discharge from all major tributaries of the typical wet (1996) and dry years (2001).

$$E = \begin{cases} M \left(\frac{\tau_b}{\tau_e} - 1 \right), & \tau_b > \tau_e \\ 0, & \tau_b \leq \tau_e \end{cases} \quad (4)$$

where, M is an empirical constant with the same unit as E and τ_e is the critical shear stress for erosion. τ_b is the bed shear stress. In this study, constant values of empirical parameters of $M = 3 \times 10^{-3} \text{ gm}^{-2}\text{s}^{-1}$ and $\tau_e = 0.05 \text{ Nm}^{-2}$ were used within the model domain (Feng et al., 2015; Moriarty et al., 2020). Assuming all particulate material with different settling velocities will be mixed together on the seabed, the critical shear stress was set as the same for all case studies to evaluate the influence of settling velocity.

The deposition rate is calculated as (Cercio et al., 2013)

$$D = \begin{cases} w_s C_b \left(1 - \frac{\tau_b}{\tau_d} \right), & \tau_b < \tau_d \\ 0, & \tau_b \geq \tau_d \end{cases} \quad (5)$$

where, C_b is the material concentration at the bottom water layer. $\tau_d [= 0.035 \text{ Nm}^{-2}]$ is the critical shear stress for deposition (Gong & Shen, 2010), below which the material settles to the bottom sediments.

At the seabed, the particulate material is allowed to settle and be re-entrained into suspension. For simplicity, only one sediment layer and no decay or burial were considered in the model. Ignoring bedload transport, the mass per unit area on the seabed C_s varies according to

$$\frac{\partial C_s}{\partial t} = D - E \quad (6)$$

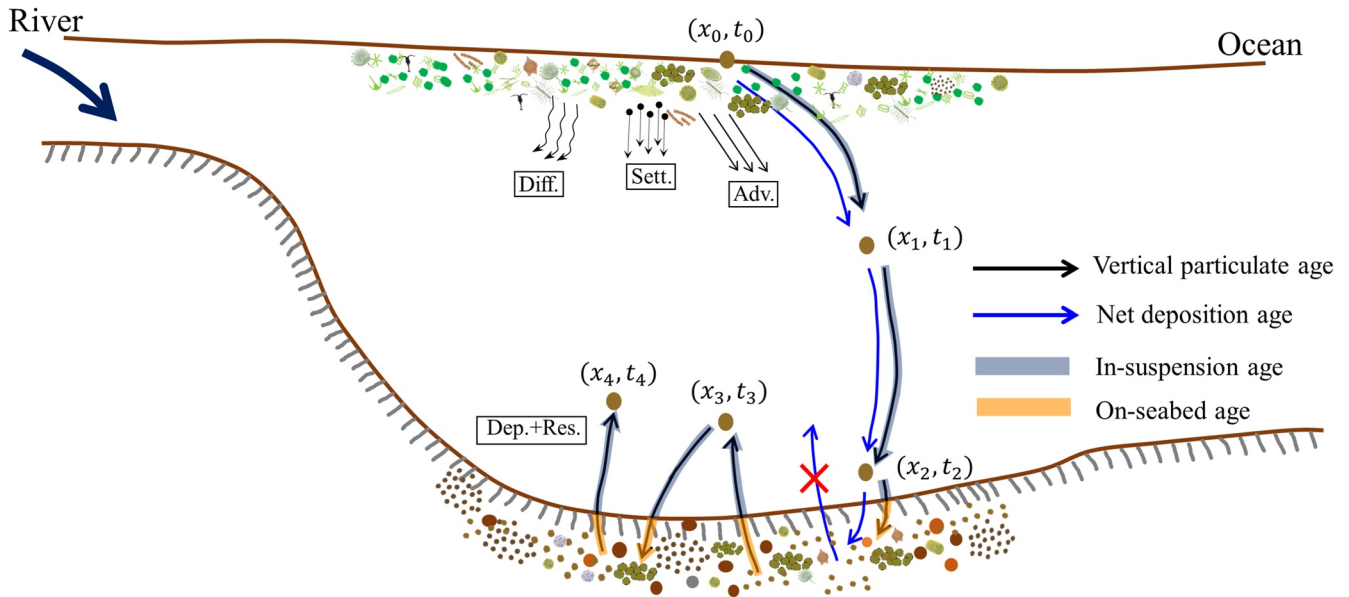


Figure 2. Schematic illustration of the vertical particulate age (the black lines, which equals to in-suspension age + on-seabed age) and the net deposition age (blue lines). The red cross mark denotes no resuspension from the seabed for the net deposition age. The gray shadows denote the “in-suspension age,” while the orange shadows denote the “on-seabed age.” Several processes influence the transport pathways of particulate material, including advection, settling, diffusion, resuspension, and deposition. Symbols courtesy of the Integration and Application of Maryland Center for Environmental Science (<https://ian.umces.edu/media-library/symbols/>).

For dissolved material, the deposition rate, erosion rate, and settling velocity are zero.

2.2. Transport Age

To characterize the timescale of particulate material transport, we modified the age calculation in EFDC that was previously used to track the chronology of water parcels (Hong & Shen, 2013) by incorporating settling, resuspension, and deposition (Figure 2). The CART framework introduces an age concentration that is treated exactly as the tracer concentration, but with a source term (“ C ” in Equation 7 given below), indicating the coupling with the tracer concentration and accounting for the aging process (Delhez & Wolk, 2013). The age concentration in the water column is

$$\frac{\partial \alpha}{\partial t} + \frac{\partial(\alpha u)}{\partial x} + \frac{\partial(\alpha v)}{\partial y} + \frac{\partial \alpha (w - w_s)}{\partial z} = \frac{\partial}{\partial x} \left(K_h \frac{\partial \alpha}{\partial x} \right) + \frac{\partial}{\partial y} \left(K_h \frac{\partial \alpha}{\partial y} \right) + \frac{\partial}{\partial z} \left(K_z \frac{\partial \alpha}{\partial z} \right) + C \quad (7)$$

where, α is the age concentration and C is the tracer concentration in Equation 1. The mean age A can be estimated as the ratio of the age concentration to the tracer concentration

$$A = \frac{\alpha}{C} \quad (8)$$

On the seabed, the age concentration is

$$\frac{\partial \alpha_s}{\partial t} = C_s + D_\alpha - E_\alpha \quad (9)$$

where, D_α and E_α in the above budget equation denote the deposition and erosion fluxes of age concentration. These fluxes account for the exchange of age content between the water column and the seabed. The material settles on the seabed with its age and is resuspended with the mean age of the material on the seabed (Ralston & Geyer, 2017),

$$D_\alpha = A_b D = \frac{\alpha_b}{C_b} D \quad (10)$$

Table 1
Definitions of All Transport Age

Terms	Definition	Notes
Vertical particulate age (VPA)	Time elapsed since the particulates last contact the surface layer. The transport process includes settling, deposition, and resuspension.	VPA = In-suspension age + On-seabed age
In-suspension age	Total time for the particulates spent in the water column since leaving the surface layer.	$C_s = 0$ in Equation 9
On-seabed age	Total time for the particulates spent in the sediments since leaving the surface layer.	$C = 0$ in Equation 7
Net deposition age	Time elapsed within the water column since the particulates leave the surface and deposit to the sediments for the first time.	$E = 0$ in Equations 3, 4, 6, and 11 $E_\alpha = 0$ in Equations 9, 11, and 12
Vertical dissolved age (VDA)	Time elapsed since the dissolved material last contacts the surface layer; No settling, deposition, and resuspension is included.	$w_s = 0$ in Equations 1–3, 5, and 12 $E = 0$ in Equations 3, 4, 6, and 11 $D = 0$ in Equations 3, 5, 6, and 10 $E_\alpha = 0$ in Equations 9, 11, and 12 $D_\alpha = 0$ in Equations 9, 10, and 12

$$E_\alpha = A_s E = \frac{\alpha_s}{C_s} E \quad (11)$$

where, A_b (α_b), A_s (α_s) are the age (age concentration) at the bottom water layer and on the seabed, respectively. The bottom boundary condition that couples Equations 7–11 is

$$w_s \alpha + K_z \frac{\partial \alpha}{\partial z} = D_\alpha - E_\alpha \quad (12)$$

To compute the vertical transport age, conservative tracers were continuously released throughout the entire surface layer of the bay (i.e., source region), excluding the grid cells outside the bay mouth (Figure 1a). At the surface, the boundary conditions are specified as $C(t, x, y, z) = 1$ and $\alpha(t, x, y, z) = 0$, and thus the VPA was reset to zero at the source region and continued aging with each model time step both in the water column and on the seabed after deposition. To further understand the dynamics of particulate material transport, the concept of age is adapted to quantify specifically (a) the time spent in the water column (“in-suspension age”, gray-shaded black lines in Figure 2) and (b) the time spent on the seabed (“on-seabed age”, orange-shaded black lines in Figure 2; Delhez & Wolk, 2013). Age can be understood as the time recorded by a virtual clock attached to a particle that starts running when the particle enters the domain of interest. To quantify the on-seabed age, the clock starts only when the particle deposits to the sediments and stops when the particle is resuspended, that is, keeping C_s in Equation 9 but setting $C = 0$ in Equation 7. In contrast, the in-suspension age, ignoring the resting phases on the seabed, can be quantified by starting the clock only when the particle is suspended, that is, keeping C in Equation 7 but setting $C_s = 0$ in Equation 9. Theoretically, the time elapsed since the particulates leave the surface layer where the VPA = 0 is the sum of the time spent in the water column (in-suspension age) and the time spent in the sediments (on-seabed age). The calculation of in-suspension age and on-seabed age by means of the virtual age clock is similar to partial age (Mouchet et al., 2016).

Additional sensitivity studies of no resuspension ($E = 0$ in Equations 3, 4, 6, and 11 and $E_\alpha = 0$ in Equations 9, 11, and 12; Table 1) were performed to investigate the influence of the resuspension process on the vertical transport age. This age is called “net deposition age,” which only tracks the time elapsed within the water column since the particulates leave the surface and deposit to the seabed for the first time (blue lines in Figure 2).

2.3. Model Setup

This study aims to evaluate the vertical transport timescale of the surface-originated particulate material under different settling velocities and freshwater discharge conditions. The years of 1996 and 2001, the typical high flow and low flow years, respectively (Harding et al., 2016, Figure 1) were chosen to investigate the impact of freshwater on the VPA. The settling velocities used in the biochemical models in CB range from 0.1 m/day to 20 m/day, with material size varying from small phytoplankton to large detritus and aggregates (Feng et al., 2015; Moriarty et al., 2020; J. Wang & Hood, 2020). The effective sinking velocity for phytoplankton in CB based on observed Chl-a concentration is 1.0–1.5 m/day (Hagy et al., 2005). Therefore, four representative settling

velocities (0, 1, 3, and 10 m/day) were applied in the present model to characterize the common groups of particulate material produced in CB. The zero settling velocity represents the dissolved material and the associated vertical transport timescale is “vertical dissolved age (VDA)” in contrast to the VPA (Table 1).

We assumed that initially no material was presented in the water column and on the seabed as we are more interested in the transport process of the newly produced POM from the primary production. The clock started once the tracer was released from the surface layer. The erosion rate E was limited by the available material on the seabed at each time step. A 60-s time step was used for both hydrodynamic and tracer simulations. The tracer concentration and age concentration were averaged daily for further analysis. Each case was cyclically run for 10 years (Shen & Wang, 2007). Specifically, the model was first run starting with the initial conditions from 1 January 1996, until 31 December 1996. The simulated age concentration and tracer concentration in the water column and on the seabed from 31 December 1996 were then used to restart the model on 1 January 1996, and the model was run until the end of 1996 again. The restart file was updated every year. In total, this one-year run was conducted ten times to ensure the model has spun up adequately. The in-suspension age can reach the equilibrium within 2–3 recycle runs, yet the on-seabed age will continue to grow as the model runs but the increasing trend gradually decreases to approach the dynamic equilibrium. Thus, all case studies were stopped at the tenth year and the results at the last year were used for diagnostic study of the VPA for particulate material in CB.

3. Results

3.1. Vertical Transport Age for Dissolved and Particulate Material

The representative results from the case with $w_s = 1$ m/day in the wet year was presented here to illustrate the marked differences in the vertical transport age between the dissolved (i.e., VDA) and particulate material (i.e., VPA; Figure 3). The potential influence of settling velocity and freshwater discharge will be addressed below. The VDA is characterized by distinct seasonality (Figures 3a–3d, and Figures 4a and 4b), with the greatest value of 28–29 days during the most stratified summer and autumn in the deep channel of the mid-bay, where the phytoplankton productivity and biomass are the highest and the summer oxygen depletion is the most extensive (Malone et al., 1988).

The horizontal distributions of the VDA and VPA share similar patterns in the regions from the bay mouth to the Rappahannock River mouth (Figure 3, location of the Rappahannock River is shown in Figure 1a), which is generally characterized by strong wave and current-induced shear stress (Moriarty et al., 2020) and vigorous water efflux and reflux (Xiong et al., 2021a). Yet a considerable increase in the VPA can be observed in the middle to the upper bay after incorporating settling and the instantaneous resuspension and deposition processes into the downward transport of particulate material (Figures 3e–3h). The horizontal pattern of the VPA also reverses between the shallow and deep water compared to the VDA in these regions. In particular, the shallow flanks have much higher VPA than the deep channel, which has fast tidal currents (Xiong et al., 2021b) and strong shear. The higher VPA over the shallow flanks corresponds to the low resuspension frequency (regions shown in Moriarty et al., 2020), resulting in the lengthy material retention on the seabed. Once the deposited material was resuspended, it provides a source of old material contributing to the increased VPA in the water column.

Moreover, a surge in the VPA was found in the upper bay (Figure 4c) following a large flood event (Figure 1b, Days 20–30 since the start of 1996), associated with the increased bottom shear stress (Figure 4e). Such an enormous flood event resulted from a record snowfall followed by a drenching rain (Sanford et al., 2001). It delivered $\sim 9 \times 10^9$ m³ of freshwater entering the bay from the Susquehanna River in approximately two weeks (Zynjuk & Majedi, 1996). Some other flood events also occurred this year, for example, the second freshwater pulse around Day 250 (Figure 1b), yet only the strong long-lasting one can cause a detectable response in the VPA. The surge of VPA in the upper bay in response to the spring freshwater pulse was also observed in the dry year of 2001 (Figure 4d). Instead, the freshwater pulse induces little variations in the VDA (Figures 4a and 4b), which is demonstrated by the sensitivity experiments in Hong and Shen (2013). Generally, the VPA is similar in both wet and dry years (Figures 4a–4d) but highly depends on the settling and resuspension process. As will be shown below, the VPA becomes less responsive to the freshwater discharge (i.e., reduced seasonality) as the settling velocity increases.

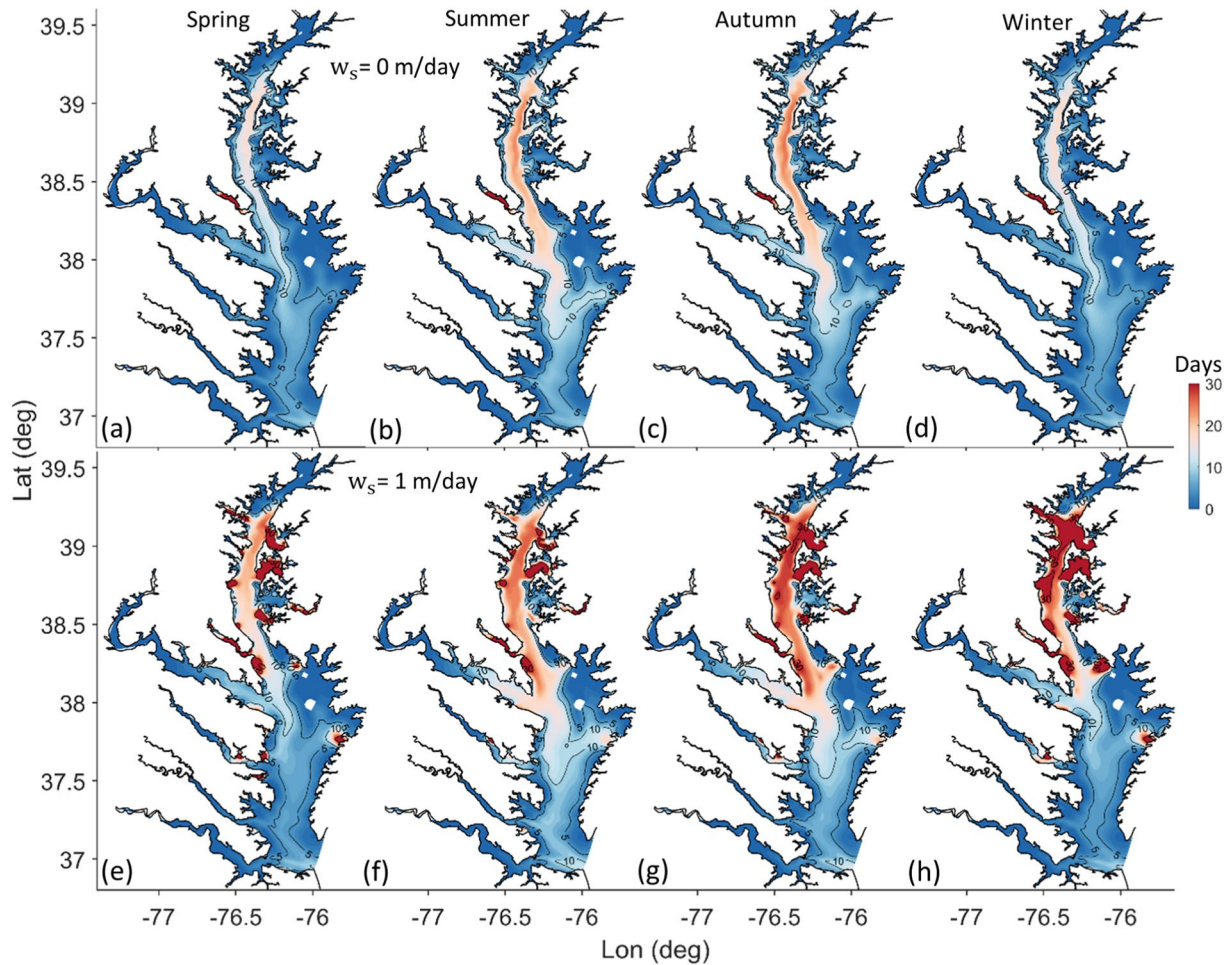


Figure 3. Seasonal variations of (a)–(d) the vertical dissolved age (days) and (e)–(h) the vertical particulate age (days) at the bottom water layer in the wet year 1996. Spring covers March to May, while summer covers June to August, autumn covers September to November, and winter covers December to February.

3.2. Total Time Spent in the Water Column and on the Seabed

Though sinking faster than the dissolved material, the much higher VPA for the particulate material at the bottom water layer, as shown above, encourages further analysis on the causes of the differences, which can be understood by partitioning the VPA into in-suspension age and on-seabed age (Figures 5 and 6). As the wet and dry years share very similar spatiotemporal patterns in the VPA, only the results of the wet year were shown hereinafter. It can be seen that the slow-sinking material ($w_s = 1$ m/day) was suspended for the longest time in the middle channel during summer and autumn due to the persistent stratification (Figures 5a–5d). The slow-sinking material stays in suspension (e.g., ~25 days in the middle bay for $w_s = 1$ m/day) longer than the fast-sinking material (e.g., ~20 days for $w_s = 3$ m/day) as is commonly expected. The in-suspension age decreases and the seasonality diminishes as the sinking rate increases (Figures 5, 6a, and 6b). It is noted that a center with high in-suspension age was located in the upper bay around 38.9–39.1°N (Figures 5e–5h) within the estuarine turbidity maximum (ETM) zone, indicating the localized efficient particle trapping capacity (Geyer, 1993; Lee et al., 2012; Sanford et al., 2001). The physical-induced entrapment of particles and aggregation of foods in ETM tend to enhance the biomass and production potential of plankton and fish (Boynton et al., 1997; North et al., 2005; North & Houde, 2001).

The longitudinal distributions of the yearly mean in-suspension age and on-seabed age were shown in Figures 6c and 6d. The distinct increase in the VPA for $w_s = 1$ m/day induced by the large flood event is also indicated as the peak in the upstream around 39.1–39.2°N in Figure 6c. Interestingly, the freshwater pulse has a weak impact on the in-suspension age (the same phenomenon observed for the VDA, Figure 4a). Instead, it induces an obvious

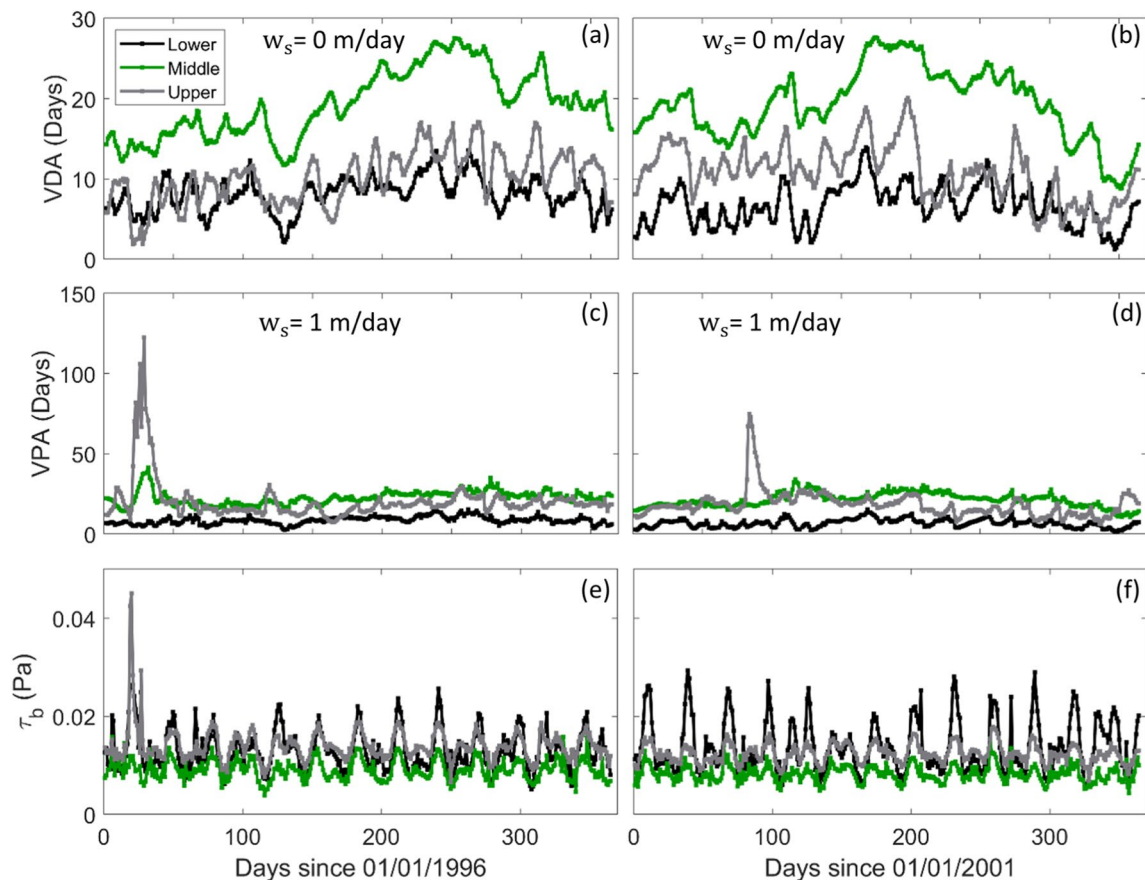


Figure 4. Time series of the daily (a)–(b) vertical dissolved age (days) and (c)–(d) vertical particulate age (days) at the bottom water layer. (e)–(f) Daily averaged current-induced bottom shear stress. All variables were averaged over the lower, middle, and upper reach of the main channel (Figure 1a).

increase in the on-seabed age. The in-suspension age mainly depends on the intensity of stratification and the properties of the material, for example, settling velocity and erodibility. As the bay is already buffered with a large amount of freshwater, the effects of springtime discharge pulse tend to diminish after several months of adjustment (Hong & Shen, 2013), thus the freshwater pulse has a minor influence on the in-suspension age on an annual scale.

For the on-seabed age, the clock turns on when the particulate material reaches the bottom sediments and turns off when it is resuspended. As age is a mass-weighted average of the newly settled material and the material deposited earlier on the seabed, the distinct increase in the on-seabed age during the strong freshwater pulse is postulated to be induced by the delivery of the much older material resuspended from the lateral depositional shallow shoals (Figure S1 in Supporting Information S1). For the case of $w_s = 3$ m/day, the annual-averaged on-seabed age in the middle bay is about 120 days (Figure 6d), suggesting that the POM deposited after the spring phytoplankton blooms contributes to the SOD and supports the phytoplankton growth in summer via the recycled nutrients (Testa & Kemp, 2008). Note that the age calculations only quantify the new material input from the surface, independent of the material on the seabed before the start of the simulation which may be much older (Ralston & Geyer, 2017). For our simulation, the maximum material age in the sediment should be smaller than the total simulation period, that is, 10 years.

In the high shear stress regions along the mainstem bay, such as downstream of the Rappahannock River mouth (Figure 1a), material may retain in the sediments shortly at the slack tides but then is resuspended without much long-term deposition. Therefore, the percentage of in-suspension age to the VPA can reach up to 99% in the lower bay especially for the slow-sinking material (Figures 6c and 6e). In contrast, the fast-sinking material can remain on the seabed and the on-seabed age accounts for 90% of the VPA in the mid-bay (Figures 6d and 6e), contributing to the high sedimentary OM content in this region besides the locally high production of OM from the spring

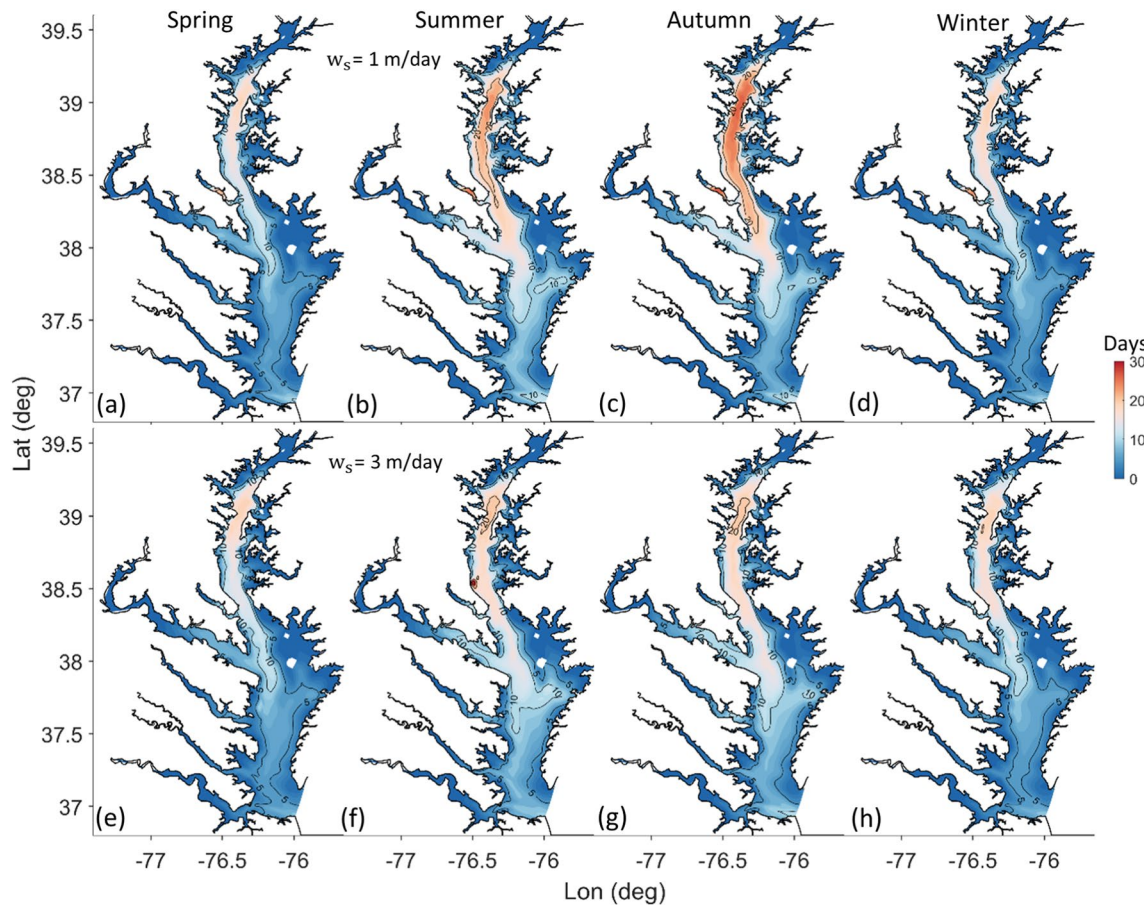


Figure 5. Seasonal variations of the in-suspension age (days) at the bottom water layer for the wet year 1996, (a)–(d) $w_s = 1$ m/day and (e)–(h) $w_s = 3$ m/day.

phytoplankton bloom (Testa et al., 2020). Moreover, the reported limited nitrogen and carbon accumulation in the sediments in the polyhaline reach of CB could also be explained by the short retention time for particulate material in the sediments in the dynamic lower bay besides the locally low phytoplankton biomass and distant fluvial sources (Testa et al., 2020).

4. Discussion

4.1. Influence of Settling Velocity on Vertical Transport Age

Settling velocity is an important property for both inorganic and organic particles. For example, the rapid-settled large particles were more effectively trapped in the ETM (Sanford et al., 2001). Small algae species enter the pelagic food chains more easily than the large species, which sink faster to the bottom and more likely enter the benthic food chains (Malone & Chervin, 1979). The process of surface OM settling to the bottom can effectively lengthen the material retention time in a system, allowing decomposition or sequestration before it might otherwise be flushed out (Hopkinson & Vallino, 1995). The settling velocity of the POM in the ocean features a wide range, from <1 m/day to >100 m/day based on field measurements (Stemmann et al., 2004; Turner, 2015). The reported algal settling velocity typically ranges from 0.1 to 5 m/day (Cercó, 2000), as a function of the algal size, shape, density, behavior, flocculation processes (Heaney & Eppley, 1981; Hutchinson, 1967; Moore & Villareal, 1996), and the algal buoyancy regulated by nutritional status and light intensity (Bienfang et al., 1982; Richardson & Cullen, 1995; Waite et al., 1992).

In this study, the settling velocities of 0, 1, 3, and 10 m/day were selected to characterize the vertical transport time for different classes of dissolved and particulate material. It is found that the VPA is rather sensitive to the variations of settling velocity. As the settling velocity increases from 0 to 10 m/day, the VPA at the bottom water

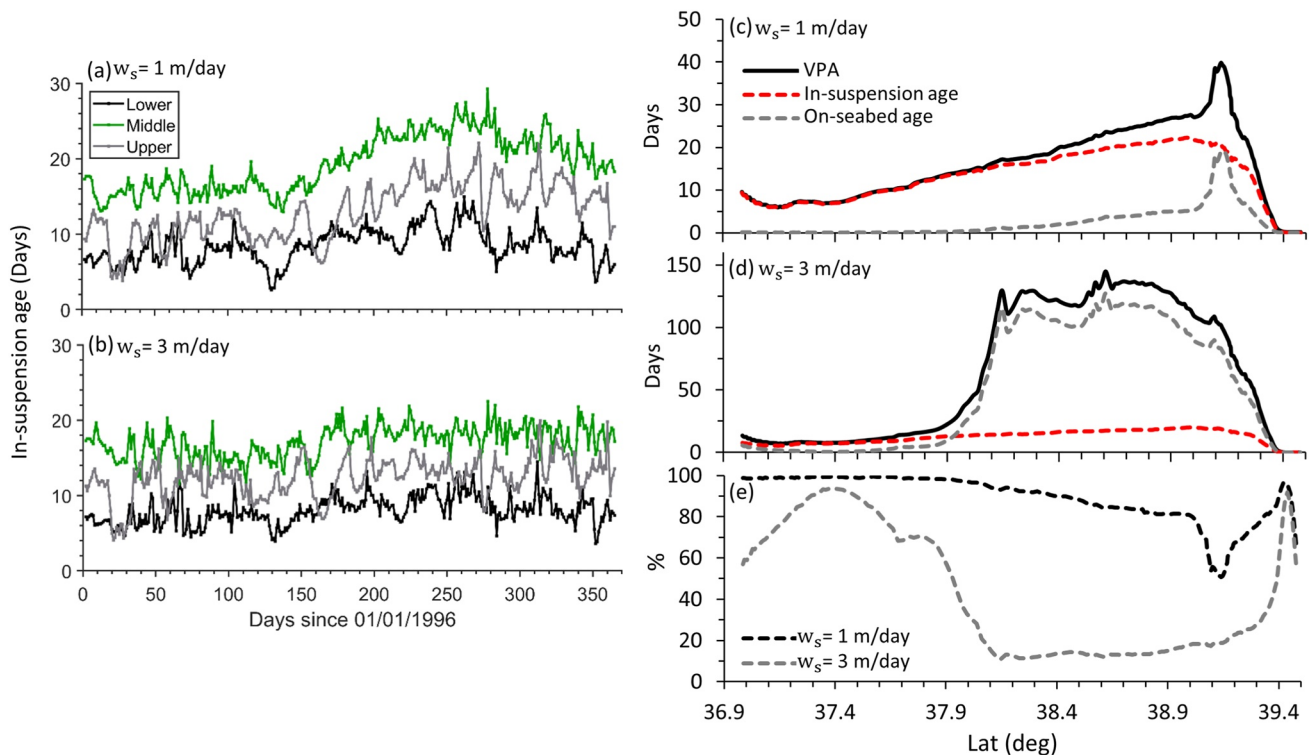


Figure 6. (a) and (b) Time series of regional-averaged daily in-suspension age (days) at the bottom water layer for $w_s = 1$ m/day and $w_s = 3$ m/day in the wet year 1996. (c) and (d) Longitudinal distributions of the yearly mean vertical particulate age (VPA; days), in-suspension age (days), and on-seabed age (days) at the bottom water layer. (e) Longitudinal variations of the percentage of in-suspension age to the VPA.

layer increased ~ 2 orders of magnitude in the middle bay (Figures 7 and 8) due to the low resuspension frequency (Moriarty et al., 2020), the elongated retention time on the seabed, and the contributions from the resuspended aged seabed material (Figure S1 in Supporting Information S1). In the dynamic lower bay, the sensitivity of the VPA to w_s decreases as the patterns of VPA are close among these cases (Figures 7 and 8). Modeling studies in the York River (Gong & Shen, 2010) and the Hudson River (Ralston & Geyer, 2017) also found that the sediment

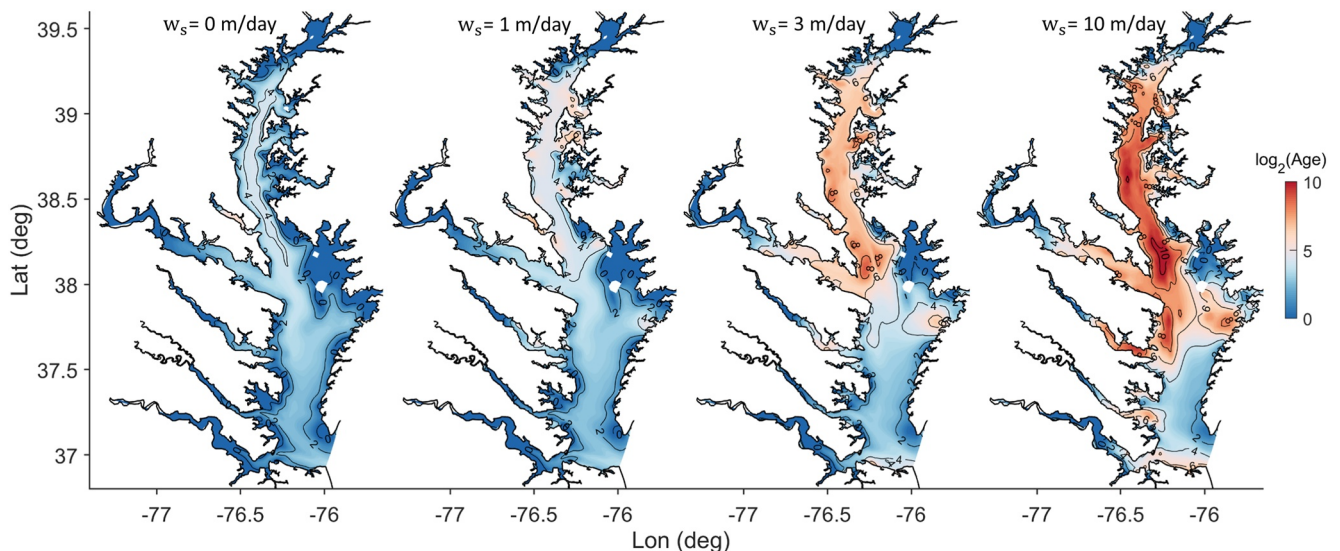


Figure 7. Yearly mean vertical dissolved or particulate age (days) at the bottom water layer for the cases with different settling velocities in the wet year 1996. The values are scaled by logarithm base 2 for better visualization.

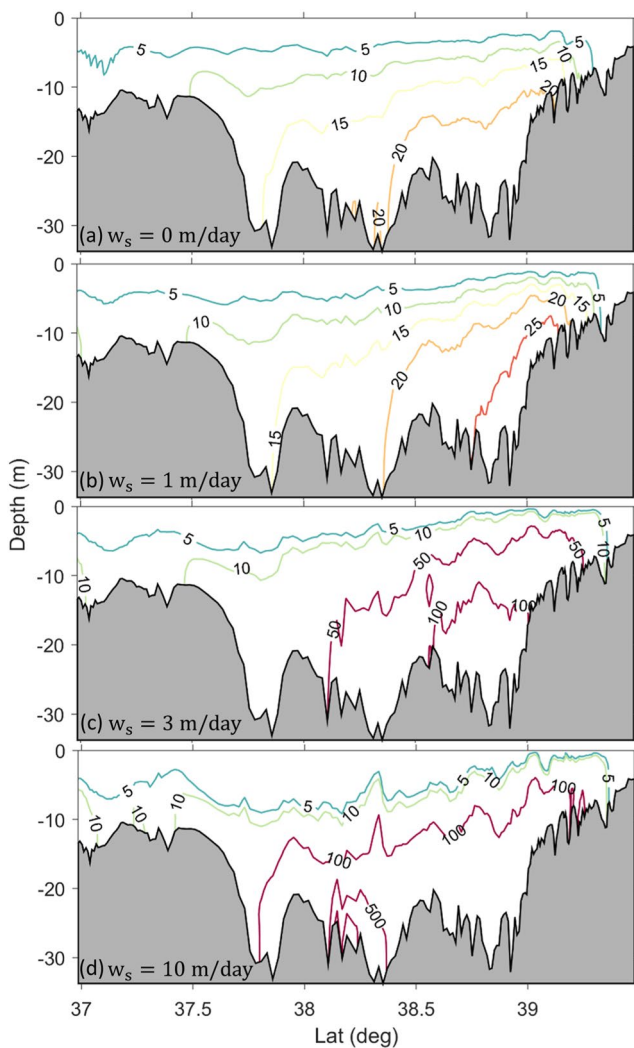


Figure 8. Along-channel contour plots of vertical dissolved or particulate age (days) for different settling velocities in summer (June–August 1996).

transport age with sources from the watershed is sensitive to the settling velocity, with increased transport time for sediment to travel from the upstream to the mouth when settling velocity is large as faster sinking leads to higher rates of deposition and slower rates of transport outward.

For the vertical transport, the fast-sinking material settles to the seabed quicker than the slow-sinking counterpart and has elongated total deposition time on the seabed. Material with the fastest sinking rate (10 m/day) in the present case studies has a VPA of over 500 days in the bottom water layer of the middle bay (Figure 8d), much longer than the in-suspension age that excluding the time spent on the seabed (~ 10 days in Figures 11c below). Given such a long period of resting on the seabed and the quick settling, the fast-sinking particulate material is more closely associated with the localized (less downstream or upstream transport) benthic biochemical cycles against the slow-sinking material that can be suspended in the water column for a lengthy duration and is more prone to grazing, entering the pelagic food chain potentially over a wider spatial extent, and contributing to the pelagic biochemical cycles. Additionally, the fast-sinking particulate material may have higher critical shear stress for erosion (although we assume all sinking materials will be well mixed on the seabed and used the same critical shear stress to focus on the influence of settling velocity), requiring stronger shear for erosion and allowing more time to stay on the seabed. Higher critical stress also indicates less frequent interactions between the water column material and the aged seabed material.

Moreover, previous studies suggest the connection of summertime hypoxia and the accumulation of OM in the bottom water during the springtime (Cercó, 2000; Kemp & Boynton, 1984; Malone et al., 1988; Zheng & DiGiacomo, 2020; Zimmerman & Canuel, 2001). Synthesizing the satellite-derived and field measurement data, Zheng and DiGiacomo (2020) argue that the bottom DO in May–July is optimally correlated with the Chl-a which was averaged covering 12–17 weeks before the present DO sampling, indicating the cumulative effects of the surface Chl-a on the bottom DO depletion. Substantial phytoplankton biomass accumulations from the winter-spring bloom are associated with low grazing rates (White & Roman, 1992) and high deposition rates of fresh OM (Kemp et al., 1999). Large pools of POM from spring blooms and the elevated temperatures in summer can enhance the water column respiration. In the sediment flux model, the rapidly reactive or labile carbon had a decay rate of 0.035 day^{-1} at 20°C , indicating a 20-day

half-life and 90% of the labile carbon being remineralized in 65 days (Brady et al., 2013; Cercó, 2000; Z. Wang et al., 2020). The estimated VPA (Figures 8b and 8c) and on-seabed age (Figures 6c and 6d) in the present study for the surface-originated particulate material is about 1–3 months for $w_s = 1\text{--}3 \text{ m/day}$ in the deep channel of the middle bay, close to the time lag between the spring blooms and the summer hypoxia. For the particulates with larger settling velocity and much longer VPA, it suggests that these materials either have been totally decomposed or are refractory which contribute little to the water column hypoxia even they are resuspended. Therefore, the transport timescale provides useful information to evaluate biochemical reactions. However, the exact number of the VPA must be interpolated with caution due to the simplifications assumed in the model and the varying hydrodynamic conditions.

Note that the VPA is different from the rather old radiocarbon age (Ralston & Geyer, 2017). The VPA calculated here represents the transport time of dissolved or particulate material generated at the surface in the estuary, rather than the much older age of organic carbon (e.g., hundreds to thousands of years B.P. in CB, Canuel & Hardison, 2016) as measured by the natural radioactive and stable isotopes of carbon (Raymond & Bauer, 2001a). Such an old age of organic carbon mainly depends on the characteristics of various carbon pools and the transport processes (Bao et al., 2019; Canuel & Hardison, 2016; Marwick et al., 2015; Raymond et al., 2004).

4.2. Important Control of Resuspension Process on the Vertical Particulate Age

Seabed resuspension processes affect water quality by altering light attenuation, primary productivity, and OM remineralization. Moriarty et al. (2020) quantify the degree to which sediment resuspension affects estuarine biochemistry in CB. They found that resuspension decreased oxygen by ~25% and increased ammonium by ~50% for the bottom water layer over the channel. Net settling velocity (or net deposition without instantaneous resuspension) is commonly used in the water quality models to represent the long-term difference between settling and resuspension processes (Cercio et al., 2010). For such application, the material will stay in the sediment permanently once settled. However, it is suggested that the net settling potentially overestimated the benefits of solids load reductions, which might be negated by continuous resuspension of particulate material already in the bay (Cercio et al., 2010).

To diagnose the impact of resuspension process on the VPA, the resuspension was turned off to represent the net deposition (blue lines in Figure 2). Figures 9 and 10 show the horizontal and along-channel distributions of the net deposition age, respectively. It can be seen that without resuspension, the net deposition age decreases greatly compared to the VPA (Figure 7) or the in-suspension age (Figures 11a–11c). The net deposition age could be regarded as a part of the in-suspension age that only accounts for the transport time before the material reaches the seabed for the first time. If the material never settles to the seabed, the net deposition age equals the in-suspension age. For instance, the minor differences between the net deposition age and the in-suspension age in the region from the bay mouth to ~37.5°N for the slow-sinking cases (Figures 11a and 11b) suggest that the VPA is less influenced by the settling and resuspension processes over this dynamic region.

In addition, the even lower net deposition age for the particulate material than the dissolved counterpart is due to less downstream transport but more locally downward transport of particulate material determined by the settling (Figure 10). The slowest sinking material ($w_s = 1$ m/day) behaves more like the dissolved one and features the greatest net deposition age in the summer and autumn due to the strongest stratification (Figures 9a–9d). The seasonality diminishes gradually as the importance of settling velocity enhances (Figure 9). The fastest sinking material ($w_s = 10$ m/day) reaches the bottom water for the first time within 4 days (Figures 9i–9l, 10d). At the along-channel dimension, the estimated location of the contour with the value of H/w_s (e.g., $H/w_s = 1$ day when $w_s = 10$ m/day and $H = 10$ m) is congruent with the depth of the long-term mean pycnocline (Figure 10; Yu et al., 2020) particularly in the middle to upper bay. Although the net deposition is often utilized in the water quality model (Cercio et al., 2010), the associated net deposition age estimated here only accounts for the time before the particulate material reaches the seabed for the first time and ignores the subsequent resuspension and deposition. Therefore, the VPA, in-suspension age and on-seabed age that fully incorporate the resuspension and deposition are recommended to interpret the realistic water quality problems.

It is also noted that the location of the maximum net deposition age shifts downstream and the along-channel gradients in the net deposition age decrease with the increased settling velocity (Figure 10). For example, the maximum VDA for $w_s = 0$ m/day is around 38.5°–39°N and the peak net deposition age moved toward 37.5°–38°N for the fastest-sinking material ($w_s = 10$ m/day) as the downward transport is less controlled by the water column stratification but more by the settling velocity and likely the strong water reflux and the vigorous vertical water exchange associated with the shoaling of the deep channel (Xiong et al., 2021a). A non-dimensional coefficient ($R = 1 - \text{net deposition age}/\text{in-suspension age}$) was estimated to specify the resuspension ratio in the water column (Figures 11d–11f). Net deposition age indicates no exchange with the sediments, thus, the difference between the in-suspension age and the net deposition age can be regarded as the total resuspension time. The magnitude of the resuspension ratio indicates the degree to which the resuspended material can be kept in the water column. For the slow-sinking scenarios ($w_s = 1$ and 3 m/day, Figures 11d and 11e), small resuspension ratio dominates the lower bay and the near-surface region, indicating low retention capacity of the resuspended material. In contrast, the ETM zone features high trapping efficiency of the resuspended material. The resuspension ratio increases and the high value expands to the whole bay (mostly confined below the pycnocline; Figures 11f) as the settling velocity increases to 10 m/day since the resuspended high-sinking material is less prone to be transported outside but more likely to be kept inside the bay. The distribution of high resuspension ratio can reach to the surface over the Rappahannock Shoal (37.2°–37.5°N), consistent with the localized vigorous vertical exchange (Xiong et al., 2021a).

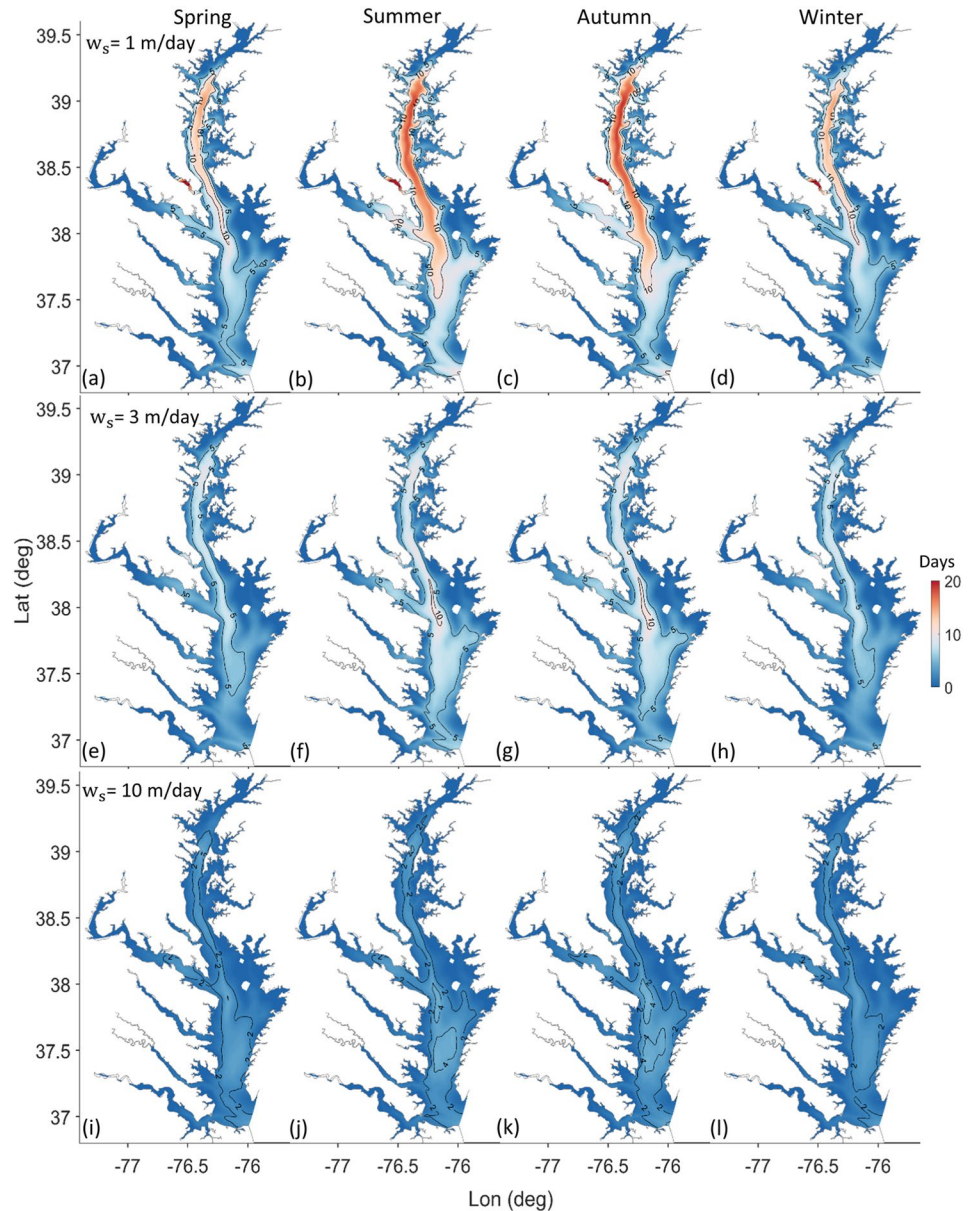


Figure 9. Horizontal distributions of the net deposition age (days) at the bottom water layer for cases with different settling velocities: (a)–(d) $w_s = 1$ m/day; (e)–(h) $w_s = 3$ m/day; (i)–(l) $w_s = 10$ m/day in the wet year 1996.

4.3. Variations of Vertical Transport Age in Wet and Dry Years

Many previous studies have examined the response of transport timescales, for example, flushing time, residence time, and water age to the various river discharge conditions. It is commonly expected that less time is required for the material (either in dissolved, particulate, or adsorbed phases) to be transported downstream under high freshwater discharge (e.g., Delhez & Wolk, 2013; Du & Shen, 2016; Gong & Shen, 2010; Shen & Haas, 2004; Zhu et al., 2020). In contrast, the VPA for the downward transport of surface-produced particulate material is less sensitive to the freshwater discharge (Figures 12c and 12d) despite that the mean flow in the wet year ($\approx 3.14 \times 10^3$ m³/s) is about 3 times the flow in the dry year ($\approx 1.04 \times 10^3$ m³/s, Figures 1b and 1c). It is mainly because the VPA is dominated by the long resting phase on the seabed as regulated by the bottom shear stress, which is close in both wet and dry years except for the higher stress in the upper bay induced by the strong discharge pulse in the wet year (Figure 12b). The along-channel stratification intensity, quantified as the maximum value of the square of Brunt Väisälä Frequency ($N^2 = g/\rho_i \partial \rho / \partial z$, where ρ_i is the water density at the depth z_i ,

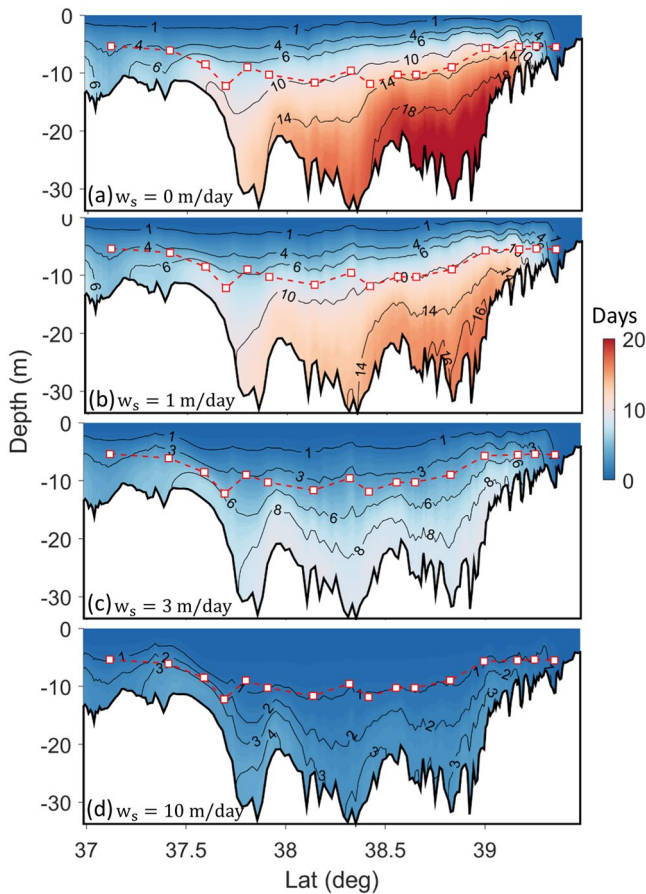


Figure 10. Along-channel distributions of (a) the yearly mean vertical dissolved age (days) and (b)–(d) the yearly mean net deposition age (days) for material with different settling velocities in the wet year 1996. The multi-year averaged pycnocline depth is denoted by the red dashed line marked with white squares.

Knauss & Garfield, 2016), is higher in the wet year particularly in the lower bay (Figure 12a), coinciding with the slightly larger net deposition age (Figure 12c) that is not subject to the controls of the seabed process. Additionally, the effect of river discharge on the VDA was discussed by Hong and Shen (2013), which shows that the pulse of river discharge has minor impacts on the summer VDA because CB is already buffered by a large amount of freshwater. The impact of the spring river discharge is also confounded by the interannual variations of the wind field (Du & Shen, 2015). Compared to the freshwater discharge, wind forcing modulates the vertical mixing more directly and rapidly, and the southerly wind strength is found to be negatively correlated with the VDA (Du & Shen, 2015). Overall, the vertical transport timescale for particulate material in CB is insensitive to the total freshwater discharge because of the large buffer of freshwater and the minor interannual variations in the bottom shear stress.

On the contrary, the episodic flood events can cause a marked increase in the VPA, for example, the VPA peak responding to the events for $w_s = 1$ m/day in both the time series in Figures 4c and 4d and the along-channel distribution in Figure 12d. Specifically, the freshwater pulse would not influence the in-suspension age but increase the on-seabed age in the main channel (Figure 6c). The on-seabed age is the weighted average of the newly delivered material and the material deposited before. The marked increase in the on-seabed age following the strong flood event is associated with the lateral transport of the much older material resuspended from the depositional shallow shoals to the deep channel as shown in Figure 13 for $w_s = 1$ m/day, Figure S2 in Supporting Information S1 for $w_s = 3$ m/day in the wet year, and Figure S3 in Supporting Information S1 for the dry year.

4.4. Limitations and Generalities

Although as the initial efforts to quantify the vertical transport age for the surface-produced particulate material in CB and to investigate its sensitivity to the important physical drivers, that is, settling velocity, resuspension process, and freshwater discharge, there are several limitations in the present model study that could be further explored. First and foremost, the possible production, decay, and transformation for POM were ignored in the age al-

gorithms. We assumed that POM is generated everywhere in the surface layer without being limited by nutrients or light, whereas the seasonal phytoplankton blooms in CB are usually patchy and the maximum Chl-a location often shifts along the mainstem (Brush et al., 2020; Harding et al., 2016). It is derived that if the decay rate of POM is constant and is independent of the transport age since it was “born” from the source region, this type of decay will not modify the age results (Deleersnijder et al., 2001). Yet it was reported that the reactivity of OM decreases with the increasing timescale as the most reactive components will be gradually lost during the transport (Catalan et al., 2016; Middelburg & Meysman, 2007). Therefore, for non-constant decay rates (e.g., the preferential utilization of the younger OM, Raymond & Bauer, 2001b) and processes associated with biochemical transformations, the transport-age based decay rates worth further efforts to be coupled with the biochemical or ecosystem models (Delhez et al., 2004). For instance, the mean age distributions of reactive inorganic soil-nitrogen were simulated by Woo and Kumar (2016, 2017) via taking into account a series of complex gain and loss processes within the nitrogen cycles.

Second, the settling velocity is spatiotemporally constant for each case study but it can change due to the size variations during the transport via biochemical reactions. For example, grazing can package small phytoplankton into large fecal pellets (Ko et al., 2003; Prahl & Carpenter, 1979). The formation of “marine snow” and large mucilaginous aggregates can also enhance the sinking rate of OM (Testa et al., 2020). The present case studies indicate the high sensitivity of the VPA to the sinking rate, thus, the potential variations in settling velocity of

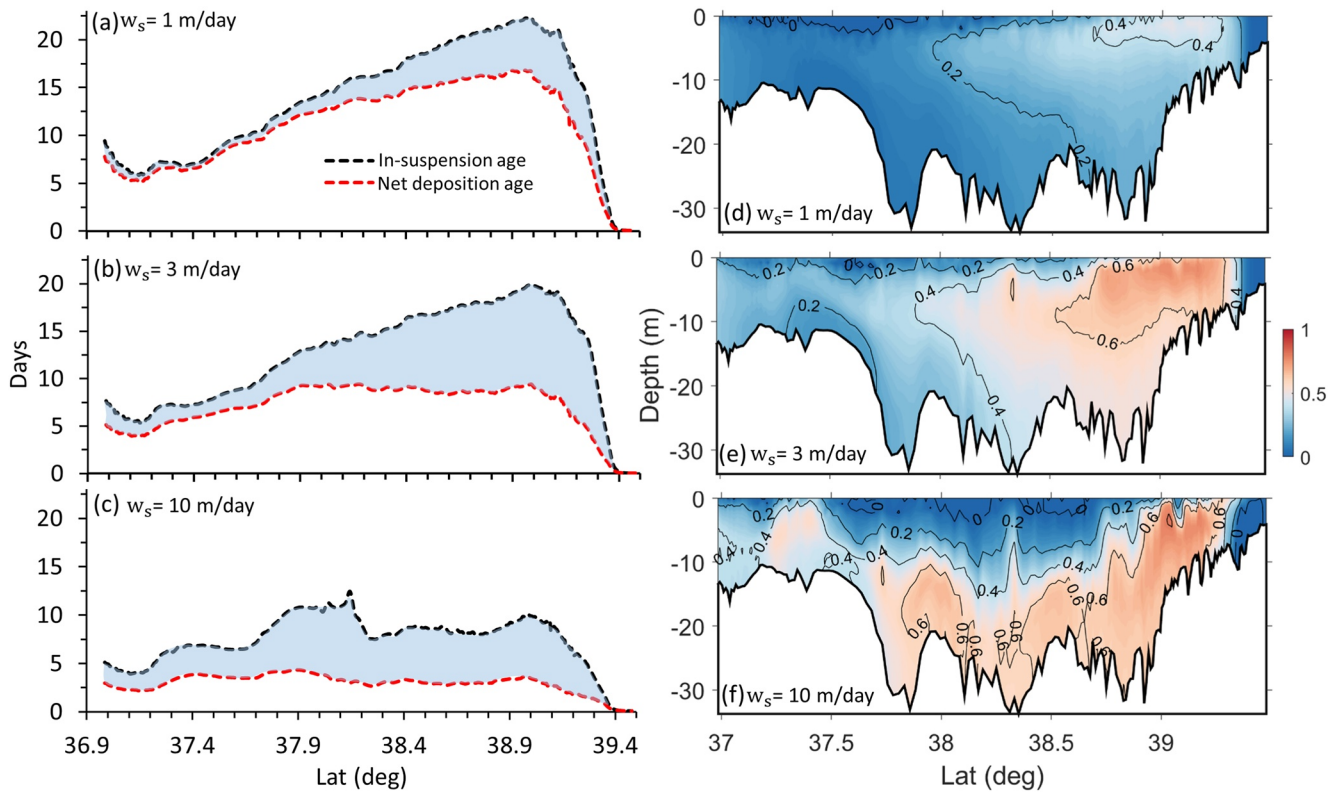


Figure 11. (a)–(c) Along-channel distributions of the yearly mean in-suspension age (days) and net deposition age (days) at the bottom water layer for different settling velocities in the wet year 1996. The light blue shadows represent the total resuspension time (= in-suspension age – net deposition age). (d)–(f) Resuspension ratio ($R = 1 - \text{net deposition age} / \text{in-suspension age}$).

particulate material during its transport might induce great differences to the estimated VPA. However, since many factors determine the sinking rate, it would be challenging and introduces large uncertainties to apply the spatiotemporally varied settling velocity.

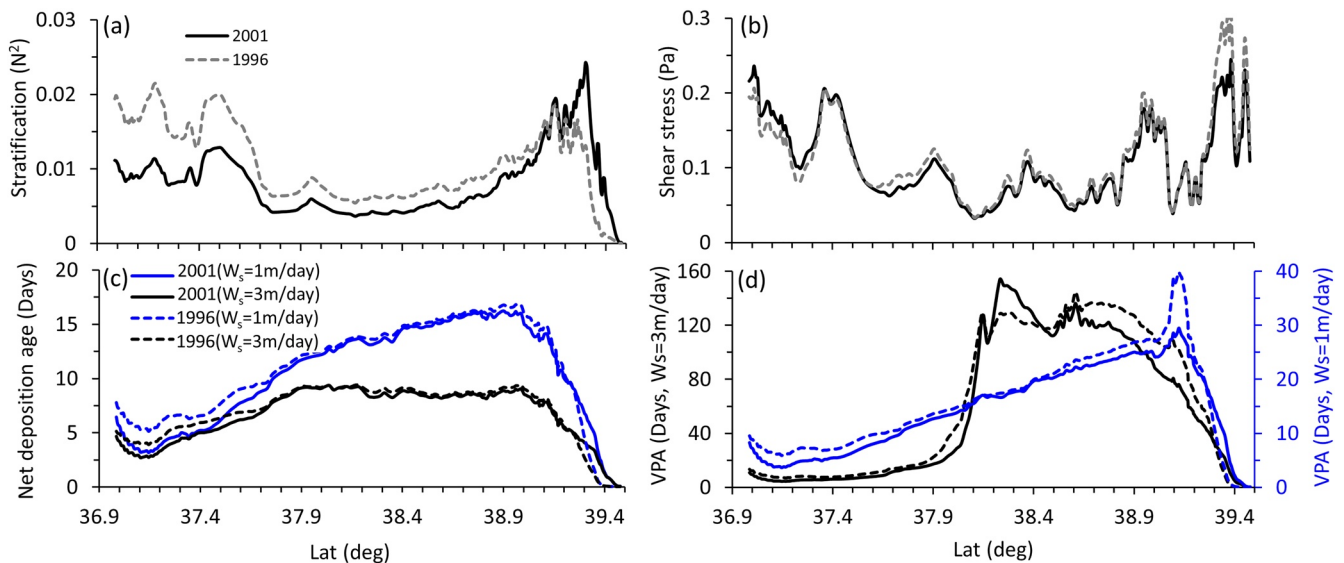


Figure 12. Along-channel distributions of (a) stratification, (b) current-induced shear stress, (c) net deposition age, and (d) vertical particulate age in wet (1996) and dry (2000) years.

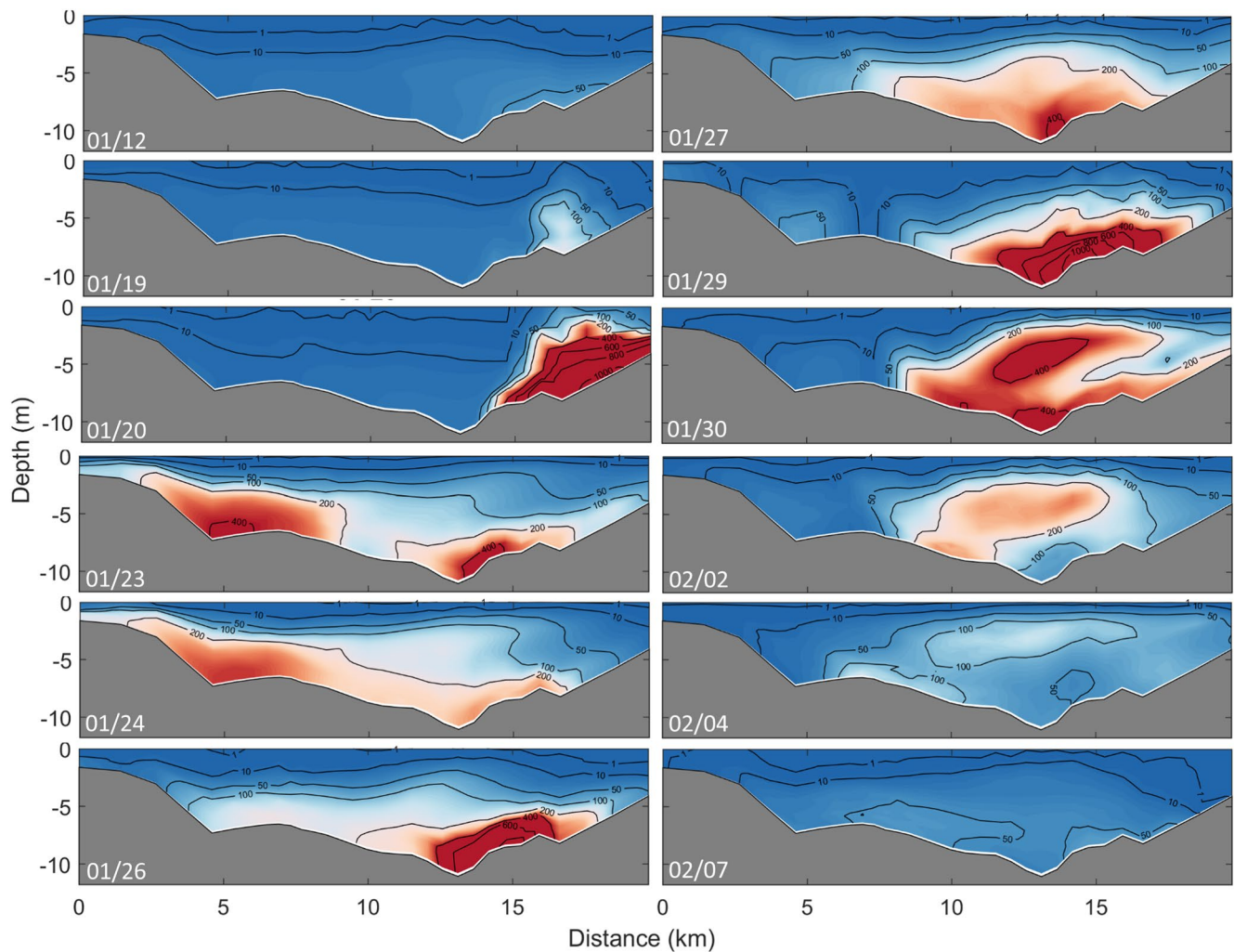


Figure 13. Evolution of the cross-bay vertical particulate age (days) for $w_s = 1$ m/day following the strong freshwater pulse of the wet year 1996. The location of the cross-bay section is shown in Figure 1.

Other limitations include the ignorance of waves and using constant critical shear stresses for erosion and deposition in the model configurations. Wave-induced shear stress and the critical shear can regulate the erosion and deposition rate and subsequently the in-suspension and on-seabed age. Waves usually play a small part in bed stresses over most CB besides during storm and wind events, especially in shallow areas (Harris et al., 2013). The critical shear stress, similar to the settling velocities, is also determined by a number of interrelated physical, biological, and chemical factors, such as grain size, sorting, density, organic composition, consolidation, and deposition history (Kimiaghalam et al., 2016; Salehi & Strom, 2012; Schaaff et al., 2002; Wiberg & Smith, 1987). As a diagnostic study to distill the first-order characteristics, we utilized the commonly used critical shear for POM in CB (Feng et al., 2015) to avoid unnecessary complexity. Furthermore, this study did not examine the multi-layer sediment model, which might affect the vertical distribution of newly deposited material and thus result in different transport time for a given size class. While the wave, critical shear stress, and the vertical distribution of material on the seabed could modulate the spatial distribution, they are unlikely to shift the overall patterns of the VPA. Although the biochemical reactions are not directly addressed in the current study, the VPA provides a common currency by which the biochemical reaction rate and physical transport timescale can be compared (Lucas & Deleersnijder, 2020; Lucas et al., 2009; Shen et al., 2013).

5. Conclusions

Accumulation and remineralization of the surface-produced POM in the bottom water layer and seabed are closely linked to hypoxia and impact the health of the aquatic ecosystems. In this study, the concept of the water age is extended to investigate the spatiotemporal variations in the vertical transport age (i.e., VPA) for particulate material originating from the surface layer. To understand the influence of settling, resuspension, and freshwater discharge on the VPA, and compare the physical transport timescales with the biochemical reactions in the water column and on the seabed, three types of age categories were calculated by controlling the virtual age clock: in-suspension age, on-seabed age, and net deposition age, to represent the transport timescale exclusively in the water column, on the seabed, and before the particulates touching the seabed for the first time, respectively. The sum of the in-suspension age and the on-seabed age is the VPA.

It was found that the VPA is much older than the VDA as the former is characterized by a long resting phase on the seabed and contributions from the resuspended aged seabed material. The VPA is rather sensitive to the settling velocity, and it varies over 2 orders of magnitude in the less-frequent resuspension environments as the settling velocity increases from 0 to 10 m/day. The ratio of the in-suspension age to the VPA decreases as the sinking rates increase. The slow-sinking material can remain in suspension for a long time especially in dynamic environments with strong bottom shear stress, thus connects more closely with the pelagic biochemical processes, while the fast-sinking material is more related to the benthic processes. The seasonality of the VPA diminishes gradually for fast-sinking material, which is mainly governed by the bottom resuspension and deposition process. The total freshwater discharge (e.g., wet and dry years) has minor impacts on the VPA, yet the long-lasting strong flood event will entrain older material from the lateral depositional shallow areas to increase the VPA in the deep channel.

The age concept provides a quantitative insight to diagnose the influence of physical processes (e.g., advection, diffusion, settling, resuspension, and deposition) on the material transport and bridges cross disciplines as the physical transport timescale and the biochemical reaction rates can be compared as a common currency (Lucas & Deleersnijder, 2020). By controlling the virtual clock, the respective time spent in different sub-domains (i.e., water column and seabed in the present study) could be estimated to further diagnose the material transport process in detail. Future improvements, such as incorporating biochemical decay or production, could be implemented to the age governing equations to better quantify the combined biophysical controls on material transport.

Data Availability Statement

Original data used for figures are available at <http://doi.org/10.5281/zenodo.4774271>.

Acknowledgments

Jilian Xiong is supported by Virginia Institute of Marine Science and Zeigler Fellowship, Norfolk Southern Fellowship, William J. Hargis, Jr. Fellowship, Dean's Fellowship, and VIMS-Commonwealth Coastal Research Fellowship. The authors would like to thank Xin Yu for providing the pycnocline data and appreciate the anonymous reviewers for the constructive suggestions and comments on the manuscript. This is Contribution No. 4075 of Virginia Institute of Marine Science, William & Mary.

References

- Bao, R., Zhao, M., McNichol, A., Wu, Y., Guo, X., Haghpor, N., & Eglinton, T. I. (2019). On the origin of aged sedimentary organic matter along a river-shelf-deep ocean transect. *Journal of Geophysical Research: Biogeosciences*, 124(8), 2582–2594. <https://doi.org/10.1029/2019JG005107>
- Bienfang, P. K., Harrison, P. J., & Quarmby, L. M. (1982). Sinking rate response to depletion of nitrate, phosphate and silicate in four marine diatoms. *Marine Biology*, 67(3), 295–302.
- Boyer, T., Levitus, S., Garcia, H., Locarnini, R. A., Stephens, C., & Antonov, J. (2005). Objective analyses of annual, seasonal, and monthly temperature and salinity for the World Ocean on a 0.25 grid. *International Journal of Climatology: A Journal of the Royal Meteorological Society*, 25(7), 931–945. <https://doi.org/10.1002/joc.1173>
- Boynton, W. R., Boicourt, W., Brandt, S., Hagy, J., Harding, L., Houde, E., et al. (1997). *Interactions between physics and biology in the estuarine turbidity maximum (ETM) of Chesapeake Bay, USA*. International Council for the Exploration of the Sea. CM 1997/S:11.
- Boynton, W. R., Ceballos, M. A. C., Bailey, E. M., Hodgkins, C. L. S., Humphrey, J. L., & Testa, J. M. (2018). Oxygen and nutrient exchanges at the sediment-water interface: A global synthesis and critique of estuarine and coastal data. *Estuaries and Coasts*, 41(2), 301–333. <https://doi.org/10.1007/s12237-017-0275-5>
- Brady, D. C., Testa, J. M., Di Toro, D. M., Boynton, W. R., & Kemp, W. M. (2013). Sediment flux modeling: Calibration and application for coastal systems. *Estuarine, Coastal and Shelf Science*, 117, 107–124. <https://doi.org/10.1016/j.ecss.2012.11.003>
- Brush, M. J., Mozetič, P., Francé, J., Aubry, F. B., Djakovac, T., Faganeli, J., et al. (2020). Phytoplankton dynamics in a changing environment. In *Coastal ecosystems in transition: A comparative analysis of the Northern Adriatic and Chesapeake Bay* (pp. 49–74).
- Canuel, E. A., & Hardison, A. K. (2016). Sources, ages, and alteration of organic matter in estuaries. *Annual Review of Marine Science*, 8, 409–434. <https://doi.org/10.1146/annurev-marine-122414-034058>
- Catalán, N., Marcé, R., Kothawala, D. N., & Tranvik, L. J. (2016). Organic carbon decomposition rates controlled by water retention time across inland waters. *Nature Geoscience*, 9(7), 501–504. <https://doi.org/10.1038/ngeo2720>
- Cerco, C., Kim, S. C., & Noel, M. (2010). The 2010 Chesapeake Bay Eutrophication Model—A report to the US Environmental Protection Agency Chesapeake Bay Program and to the US Army engineer Baltimore District. *US Army Engineer Research and Development Center, Vicksburg MS*.

- Cerco, C. F. (2000). Phytoplankton kinetics in the Chesapeake Bay eutrophication model. *Water Quality and Ecosystem Modeling*, 1(1), 5–49.
- Cerco, C. F., Kim, S. C., & Noel, M. R. (2013). Management modeling of suspended solids in the Chesapeake Bay, USA. *Estuarine, Coastal and Shelf Science*, 116, 87–98. <https://doi.org/10.1016/j.ecss.2012.07.009>
- de Brye, B., de Brauwere, A., Gourgue, O., Delhez, É. J. M., & Deleersnijder, É. (2012). Water renewal timescales in the Scheldt Estuary. *Journal of Marine Systems*, 94, 74–86. <https://doi.org/10.1016/j.jmarsys.2011.10.013>
- Deleersnijder, É., Campin, J. M., & Delhez, É. J. M. (2001). The concept of age in marine modelling: I. Theory and preliminary model results. *Journal of Marine Systems*, 28(3–4), 229–267. [https://doi.org/10.1016/S0924-7963\(01\)00026-4](https://doi.org/10.1016/S0924-7963(01)00026-4)
- Delhez, É. J. M., Campin, J. M., Hirst, A. C., & Deleersnijder, É. (1999). Toward a general theory of the age in ocean modelling. *Ocean Modelling*, 1(1), 17–27.
- Delhez, É. J. M., Lacroix, G., & Deleersnijder, É. (2004). The age as a diagnostic of the dynamics of marine ecosystem models. *Ocean Dynamics*, 54(2), 221–231. <https://doi.org/10.1007/s10236-003-0075-2>
- Delhez, É. J. M., & Wolk, F. (2013). Diagnosis of the transport of adsorbed material in the Scheldt estuary: A proof of concept. *Journal of Marine Systems*, 128, 17–26. <https://doi.org/10.1016/j.jmarsys.2012.01.007>
- Du, J., & Shen, J. (2015). Decoupling the influence of biological and physical processes on the dissolved oxygen in the Chesapeake Bay. *Journal of Geophysical Research: Oceans*, 120(1), 78–93. <https://doi.org/10.1002/2014JC010422>
- Du, J., & Shen, J. (2016). Water residence time in Chesapeake Bay for 1980–2012. *Journal of Marine Systems*, 164, 101–111. <https://doi.org/10.1016/j.jmarsys.2016.08.011>
- Feng, Y., Friedrichs, M. A., Wilkin, J., Tian, H., Yang, Q., Hofmann, E. E., et al. (2015). Chesapeake Bay nitrogen fluxes derived from a land-estuarine ocean biogeochemical modeling system: Model description, evaluation, and nitrogen budgets. *Journal of Geophysical Research: Biogeosciences*, 120(8), 1666–1695. <https://doi.org/10.1002/2015JG002931>
- Fennel, K., & Testa, J. M. (2019). Biogeochemical controls on coastal hypoxia. *Annual Review of Marine Science*, 11, 105–130. <https://doi.org/10.1146/annurev-marine-010318-095138>
- Geyer, W. R. (1993). The importance of suppression of turbulence by stratification on the estuarine turbidity maximum. *Estuaries*, 16(1), 113–125.
- Gong, W., & Shen, J. (2010). A model diagnostic study of age of river-borne sediment transport in the tidal York River Estuary. *Environmental Fluid Mechanics*, 10(1–2), 177–196.
- Gustafsson, K. E., & Bendtsen, J. (2007). Elucidating the dynamics and mixing agents of a shallow fjord through age tracer modelling. *Estuarine, Coastal and Shelf Science*, 74(4), 641–654. <https://doi.org/10.1016/j.ecss.2007.05.023>
- Hagy, J. D., Boynton, W. R., & Jasinski, D. A. (2005). Modelling phytoplankton deposition to Chesapeake Bay sediments during winter–spring: Interannual variability in relation to river flow. *Estuarine, Coastal and Shelf Science*, 62(1–2), 25–40. <https://doi.org/10.1016/j.ecss.2004.08.004>
- Hamrick, J. M. (1992). *A three-dimensional environmental fluid dynamics computer code: Theoretical and computational aspects*. Special report in applied marine science and ocean engineering, no. 317. Virginia Institute of Marine Science, William & Mary. <https://doi.org/10.21220/V5TT6C>
- Harding, L. W., Jr, Mallonee, M. E., Perry, E. S., Miller, W. D., Adolf, J. E., Gallegos, C. L., & Paerl, H. W. (2016). Variable climatic conditions dominate recent phytoplankton dynamics in Chesapeake Bay. *Scientific Reports*, 6(1), 23773. <https://doi.org/10.1038/srep23773>
- Harris, C. K., Rinehimer, J. P., & Kim, S. C. (2013). Estimates of bed stresses within a model of Chesapeake Bay. *Estuarine and Coastal Modeling (2011)* (pp. 415–434).
- Heaney, S. I., & Eppley, R. W. (1981). Light, temperature and nitrogen as interacting factors affecting diel vertical migrations of dinoflagellates in culture. *Journal of Plankton Research*, 3(2), 331–344.
- Hong, B., & Shen, J. (2012). Responses of estuarine salinity and transport processes to potential future sea-level rise in the Chesapeake Bay. *Estuarine, Coastal and Shelf Science*, 104, 33–45. <https://doi.org/10.1016/j.ecss.2012.03.014>
- Hong, B., & Shen, J. (2013). Linking dynamics of transport timescale and variations of hypoxia in the Chesapeake Bay. *Journal of Geophysical Research: Oceans*, 118(11), 6017–6029. <https://doi.org/10.1002/2013JC008859>
- Hopkinson, C. S., & Vallino, J. J. (1995). The relationships among man's activities in watersheds and estuaries: A model of runoff effects on patterns of estuarine community metabolism. *Estuaries*, 18(4), 598–621.
- Hutchinson, G. E. (1967). *A Treatise on limnology: Introduction to lake biology and the limnoplankton* (Vol. 2). Wiley.
- Kemp, M. W., & Boynton, W. R. (1984). Spatial and temporal coupling of nutrient inputs to estuarine primary production: The role of particulate transport and decomposition. *Bulletin of Marine Science*, 35(3), 522–535.
- Kemp, W. M., Faganeli, J., Puskaric, S., Smith, E. M., & Boynton, W. R. (1999). Pelagic-benthic coupling and nutrient cycling. *Coastal and Estuarine Studies*, 295–340.
- Kemp, W. M., Sampou, P. A., Garber, J., Tuttle, J., & Boynton, W. R. (1992). Seasonal depletion of oxygen from bottom waters of Chesapeake Bay: Roles of benthic and planktonic respiration and physical exchange processes. *Marine Ecology Progress Series*, 137–152.
- Kemp, W. M., Smith, E. M., Marvin-DiPasquale, M., & Boynton, W. R. (1997). Organic carbon balance and net ecosystem metabolism in Chesapeake Bay. *Marine Ecology Progress Series*, 150, 229–248.
- Kimiaghalam, N., Clark, S. P., & Ahmari, H. R. (2016). An experimental study on the effects of physical, mechanical, and electrochemical properties of natural cohesive soils on critical shear stress and erosion rate. *International Journal of Sediment Research*, 31(1), 1–15. <https://doi.org/10.1016/j.ijsrc.2015.01.001>
- Knauss, J. A., & Garfield, N. (2016). *Introduction to physical oceanography*. Waveland Press.
- Ko, F. C., Sanford, L. P., & Baker, J. E. (2003). Internal recycling of particle reactive organic chemicals in the Chesapeake Bay water column. *Marine Chemistry*, 81(3–4), 163–176. [https://doi.org/10.1016/S0304-4203\(03\)00027-6](https://doi.org/10.1016/S0304-4203(03)00027-6)
- Lee, D. Y., Keller, D. P., Crump, B. C., & Hood, R. R. (2012). Community metabolism and energy transfer in the Chesapeake Bay estuarine turbidity maximum. *Marine Ecology Progress Series*, 449, 65–82. <https://doi.org/10.3354/meps09543>
- Lucas, L. V., Thompson, J. K., & Brown, L. R. (2009). Why are diverse relationships observed between phytoplankton biomass and transport time? *Limnology and Oceanography*, 54(1), 381–390. <https://doi.org/10.4319/lo.2009.54.1.0381>
- Lucas, V. L., & Deleersnijder, É. (2020). Timescale methods for simplifying, understanding and modeling biophysical and water quality processes in coastal aquatic ecosystems: A review. *Water*, 12(10), 2717.
- Malone, T. C., & Chervin, M. B. (1979). The production and fate of phytoplankton size fractions in the plume of the Hudson River, New York Bight. *Limnology and Oceanography*, 24(4), 683–696.
- Malone, T. C., Crocker, L. H., Pike, S. E., & Wendler, B. W. (1988). Influences of river flow on the dynamics of phytoplankton production in a partially stratified estuary. *Marine Ecology Progress Series*, 48(3), 235–249.
- Malone, T. C., Kemp, W. M., Ducklow, H. W., Boynton, W. R., Tuttle, J. H., & Jonas, R. B. (1986). Lateral variation in the production and fate of phytoplankton in a partially stratified estuary. *Marine Ecology Progress Series*, 149–160.

- Marshall, H. G., Lacouture, R. V., Buchanan, C., & Johnson, J. M. (2006). Phytoplankton assemblages associated with water quality and salinity regions in Chesapeake Bay, USA. *Estuarine, Coastal and Shelf Science*, 69(1–2), 10–18. <https://doi.org/10.1016/j.ecss.2006.03.019>
- Marwick, T. R., Tammooh, F., Teodoru, C. R., Borges, A. V., Darchambeau, F., & Bouillon, S. (2015). The age of river-transported carbon: A global perspective. *Global Biogeochemical Cycles*, 29(2), 122–137. <https://doi.org/10.1002/2014GB004911>
- McCallister, S. L., Bauer, J. E., Ducklow, H. W., & Canuel, E. A. (2006). Sources of estuarine dissolved and particulate organic matter: A multi-tracer approach. *Organic Geochemistry*, 37(4), 454–468. <https://doi.org/10.1016/j.orggeochem.2005.12.005>
- Mercier, C., & Delhez, É. J. M. (2007). Diagnosis of the sediment transport in the Belgian Coastal Zone. *Estuarine, Coastal and Shelf Science*, 74(4), 670–683. <https://doi.org/10.1016/j.ecss.2007.05.010>
- Middelburg, J. J., & Meysman, F. J. (2007). Burial at sea. *Science*, 316(5829), 1294–1295. <https://doi.org/10.1126/science.1144001>
- Moore, J. K., & Villareal, T. A. (1996). Size-ascent rate relationships in positively buoyant marine diatoms. *Limnology and Oceanography*, 41(7), 1514–1520.
- Moriarty, J. M., Friedrichs, M. A., & Harris, C. K. (2020). Seabed resuspension in the Chesapeake Bay: Implications for biogeochemical cycling and hypoxia. *Estuaries and Coasts*, 1–20.
- Mouchet, A., Cornaton, F., Deleersnijder, É., & Delhez, É. J. M. (2016). Partial ages: Diagnosing transport processes by means of multiple clocks. *Ocean Dynamics*, 66(3), 367–386. <https://doi.org/10.1007/s10236-016-0922-6>
- Murphy, R. R., Kemp, W. M., & Ball, W. P. (2011). Long-term trends in Chesapeake Bay seasonal hypoxia, stratification, and nutrient loading. *Estuaries and Coasts*, 34(6), 1293–1309. <https://doi.org/10.1007/s12237-011-9413-7>
- North, E. W., Hood, R. R., Chao, S. Y., & Sanford, L. P. (2005). The influence of episodic events on transport of striped bass eggs to the estuarine turbidity maximum nursery area. *Estuaries*, 28(1), 108–123. <https://doi.org/10.1007/BF02732758>
- North, E. W., & Houde, E. D. (2001). Retention of white perch and striped bass larvae: Biological-physical interactions in Chesapeake Bay estuarine turbidity maximum. *Estuaries*, 24(5), 756–769.
- Officer, C. B., Biggs, R. B., Taft, J. L., Cronin, L. E., Tyler, M. A., & Boynton, W. R. (1984). Chesapeake Bay anoxia: Origin, development, and significance. *Science*, 223(4631), 22–27.
- Prahl, F. G., & Carpenter, R. O. Y. (1979). The role of zooplankton fecal pellets in the sedimentation of polycyclic aromatic hydrocarbons in Dabob Bay, Washington. *Geochimica et Cosmochimica Acta*, 43(12), 1959–1972.
- Rabalais, N. N., Diaz, R. J., Levin, L. A., Turner, R. E., Gilbert, D., & Zhang, J. (2010). Dynamics and distribution of natural and human-caused hypoxia. *Biogeosciences*, 7(2), 585–619.
- Ralston, D. K., & Geyer, W. R. (2017). Sediment transport time scales and trapping efficiency in a tidal river. *Journal of Geophysical Research: Earth Surface*, 122(11), 2042–2063. <https://doi.org/10.1002/2017JF004337>
- Raymond, P. A., & Bauer, J. E. (2001a). Use of ¹⁴C and ¹³C natural abundances for evaluating riverine, estuarine, and coastal DOC and POC sources and cycling: A review and synthesis. *Organic Geochemistry*, 32(4), 469–485.
- Raymond, P. A., & Bauer, J. E. (2001b). Riverine export of aged terrestrial organic matter to the North Atlantic Ocean. *Nature*, 409(6819), 497–500.
- Raymond, P. A., Bauer, J. E., Caraco, N. F., Cole, J. J., Longworth, B., & Petsch, S. T. (2004). Controls on the variability of organic matter and dissolved inorganic carbon ages in northeast US rivers. *Marine Chemistry*, 92(1–4), 353–366. <https://doi.org/10.1016/j.marchem.2004.06.036>
- Richardson, T. L., & Cullen, J. J. (1995). Changes in buoyancy and chemical composition during growth of a coastal marine diatom: Ecological and biogeochemical consequences. *Marine Ecology Progress Series*, 128, 77–90.
- Salehi, M., & Strom, K. (2012). Measurement of critical shear stress for mud mixtures in the San Jacinto estuary under different wave and current combinations. *Continental Shelf Research*, 47, 78–92. <https://doi.org/10.1016/j.csr.2012.07.004>
- Sanford, L. P., Suttles, S. E., & Halka, J. P. (2001). Reconsidering the physics of the Chesapeake Bay estuarine turbidity maximum. *Estuaries*, 24(5), 655–669.
- Schaff, E., Grenz, C., & Pinazo, C. (2002). Erosion of particulate inorganic and organic matter in the Gulf of Lion. *Comptes Rendus Geoscience*, 334(15), 1071–1077.
- Shen, J., & Haas, L. (2004). Calculating age and residence time in the tidal York River using three-dimensional model experiments. *Estuarine, Coastal and Shelf Science*, 61(3), 449–461. <https://doi.org/10.1016/j.ecss.2004.06.010>
- Shen, J., Hong, B., & Kuo, A. Y. (2013). Using timescales to interpret dissolved oxygen distributions in the bottom waters of Chesapeake Bay. *Limnology and Oceanography*, 58(6), 2237–2248. <https://doi.org/10.4319/lo.2013.58.6.2237>
- Shen, J., & Wang, H. V. (2007). Determining the age of water and long-term transport timescale of the Chesapeake Bay. *Estuarine, Coastal and Shelf Science*, 74(4), 585–598. <https://doi.org/10.1016/j.ecss.2007.05.017>
- Stemmann, L., Jackson, G. A., & Ianson, D. (2004). A vertical model of particle size distributions and fluxes in the midwater column that includes biological and physical processes—Part I: Model formulation. *Deep Sea Research Part I: Oceanographic Research Papers*, 51(7), 865–884. <https://doi.org/10.1016/j.dsr.2004.03.001>
- Sun, J., Liu, L., Lin, J., Lin, B., & Zhao, H. (2020). Vertical water renewal in a large estuary and implications for water quality. *Science of the Total Environment*, 710, 135593. <https://doi.org/10.1016/j.scitotenv.2019.135593>
- Taft, J. L., Taylor, W. R., Hartwig, E. O., & Loftus, R. (1980). Seasonal oxygen depletion in Chesapeake Bay. *Estuaries*, 3(4), 242–247.
- Takeoka, H. (1984). Fundamental concepts of exchange and transport time scales in a coastal sea. *Continental Shelf Research*, 3(3), 311–326.
- Testa, J. M., Faganeli, J., Gianni, M., Brush, M. J., De Vittor, C., Boynton, W. R., et al. (2020). Advances in our understanding of Pelagic–Benthic Coupling. In *Coastal ecosystems in transition: A comparative analysis of the Northern Adriatic and Chesapeake Bay* (pp. 147–175).
- Testa, J. M., & Kemp, W. M. (2008). Variability of biogeochemical processes and physical transport in a partially stratified estuary: A box-modeling analysis. *Marine Ecology Progress Series*, 356, 63–79.
- Turner, J. T. (2015). Zooplankton fecal pellets, marine snow, phytodetritus and the ocean's biological pump. *Progress in Oceanography*, 130, 205–248. <https://doi.org/10.1016/j.pocan.2014.08.005>
- Waite, A. M., Thompson, P. A., & Harrison, P. J. (1992). Does energy control the sinking rates of marine diatoms? *Limnology and Oceanography*, 37(3), 468–477.
- Wang, H. (2020). *A numerical investigation of variability in particulate organic matter transport and fate, phytoplankton and primary production, and denitrification in a partially mixed estuary* (Dissertation). University of Maryland. <https://doi.org/10.13016/4qtj-sulu>
- Wang, J., & Hood, R. R. (2020). Modeling the origin of the particulate organic matter flux to the hypoxic Zone of Chesapeake Bay in early summer. *Estuaries and Coasts*, 1–17. <https://doi.org/10.1007/s12237-020-00806-0>
- Wang, Z., Chai, F., & Brady, D. (2020). Development of a new sediment flux model—Application in Chesapeake Bay. *Progress in Oceanography*, 185, 102332. <https://doi.org/10.1016/j.pocan.2020.102332>
- White, J. R., & Roman, M. R. (1992). Seasonal study of grazing by metazoan zooplankton in the mesohaline Chesapeake Bay. *Marine Ecology Progress Series*, 86, 251–261.

- Wiberg, P. L., & Smith, J. D. (1987). Calculations of the critical shear stress for motion of uniform and heterogeneous sediments. *Water Resources Research*, 23(8), 1471–1480.
- Woo, D. K., & Kumar, P. (2016). Mean age distribution of inorganic soil-nitrogen. *Water Resources Research*, 52(7), 5516–5536. <https://doi.org/10.1002/2015WR017799>
- Woo, D. K., & Kumar, P. (2017). Role of micro-topographic variability on the distribution of inorganic soil-nitrogen age in intensively managed landscape. *Water Resources Research*, 53(10), 8404–8422. <https://doi.org/10.1002/2017WR021053>
- Xiong, J., Shen, J., & Qin, Q. (2021a). Exchange flow and material transport along the salinity gradient of a long estuary. *Journal of Geophysical Research: Oceans*, e2021JC017185. <https://doi.org/10.1029/2021JC017185>
- Xiong, J., Shen, J., Qin, Q., & Du, J. (2021b). Water exchange and its relationships with external forcings and residence time in Chesapeake Bay. *Journal of Marine Systems*, 215, 103497. <https://doi.org/10.1016/j.jmarsys.2020.103497>
- Yu, X., Shen, J., & Du, J. (2020). A machine-learning-Based Model for water quality in coastal waters, taking dissolved oxygen and hypoxia in Chesapeake Bay as an example. *Water Resources Research*, 56(9), e2020WR027227. <https://doi.org/10.1029/2020WR027227>
- Zhang, W. G., Wilkin, J. L., & Schofield, O. M. E. (2010). Simulation of water age and residence time in New York Bight. *Journal of Physical Oceanography*, 40(5), 965–982. <https://doi.org/10.1175/2009JPO4249.1>
- Zheng, G., & DiGiacomo, P. M. (2020). Linkages between phytoplankton and bottom oxygen in the Chesapeake Bay. *Journal of Geophysical Research: Oceans*, 125(2), e2019JC015650. <https://doi.org/10.1029/2019JC015650>
- Zhu, L., Gong, W., Zhang, H., Huang, W., & Zhang, R. (2020). Numerical study of sediment transport time scales in an ebb-dominated waterway. *Journal of Hydrology*, 591, 125299. <https://doi.org/10.1016/j.jhydrol.2020.125299>
- Zhu, L., Zhang, H., Guo, L., Huang, W., & Gong, W. (2021). Estimation of riverine sediment fate and transport timescales in a wide estuary with multiple sources. *Journal of Marine Systems*, 214, 103488. <https://doi.org/10.1016/j.jmarsys.2020.103488>
- Zimmerman, A. R., & Canuel, E. A. (2001). Bulk organic matter and lipid biomarker composition of Chesapeake Bay surficial sediments as indicators of environmental processes. *Estuarine, Coastal and Shelf Science*, 53(3), 319–341.
- Zynjuk, L. D., & Majedi, B. F. (1996). *January 1996 floods deliver large loads of nutrients and sediment to the Chesapeake Bay (No. 140-96)*. US Geological Survey.